Title
SOME CALORIMETRIC INVESTIGATIONS OP THE BOLE OF f ELECTRONS IN SUPER CONDUCTIVITY AND MAGNETISM

Author
Bader, Samuel David.

Publication Date
1974

LBL-2297

SOME CALORIMETRIC INVESTIGATIONS OF THE ROLE OF *f* ELECTRONS IN SUPERCONDUCTIVITY AND MAGNETISM

Samuel David Bader
(Ph. D. Thesis)

January 1974

Prepared for the U.S. Atomic Energy Commission under Contract W-7405-ENG-48

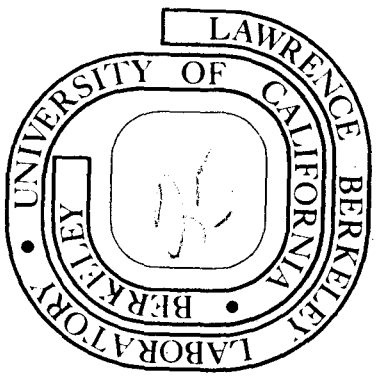

LBL-2297

DISCLAIMER

In Memory of my Brother

Peter Blake Bader

Table of Contents

PART ONE: $\underline{La},Ce)Al_2$

PART TWO: α-U

PART THREE: SmS

SOME CALORIMETRIC INVESTIGATIONS OF THE ROLE OF *f* ELECTRONS IN SUPERCONDUCTIVITY AND MAGNETISM

Samuel David Bader

Inorganic Materials Research Division, Lawrence Berkeley Laboratory
and Department of Chemistry; University of California,
Berkeley, California

ABSTRACT

PART ONE: $(La,Ce)Al_2$

The heat capacity of the system $(La,Ce)Al_2$ for 0.0, 0.193, 0.64, and 0.906 at.% Ce has been measured between approximately 0.06 and 22 K and in magnetic fields up to 38 kOe. In the normal state, there is Rln2 entropy associated with the Ce spin system and this entropy is removed in the formation of the spin-compensated state. The normal state Kondo temperature is 0.42 K. The three more-dilute samples exhibit superconductivity but cannot be described by the Bardeen-Cooper-Schrieffer or Abrikosov-Gor'kov theories. Significant low-energy excitations are evident in the superconducting state and they may be associated with quasibound states deep in the energy gap of the pure superconductor. For the 0.193 at.% Ce alloy in the superconducting state the characteristic temperature associated with Ce-spin ordering in the normal state is reduced by an estimated order of magnitude. For the 0.64 at.% Ce alloy a small, broadened superconducting anomaly appears in the heat capacity above 1 K, however, no anomaly that could be interpreted as a broadened discontinuity was found at the magnetically-detected transition back into the normal state at lower temperatures.

PART TWO: α-U

The heat capacities of five samples of α-U have been measured between approximately 0.1 and 2 K at zero pressure. The four polycrystalline samples exhibited broad, bulk superconducting transitions. The γ-values and the smearing of the superconducting transitions are sensitive to grain size--the small-grained samples had the highest γ-values and the broadest superconducting transitions. A single crystal had the lowest γ-value and appeared to be beginning to enter the superconducting state below 0.25 K. The shape of the heat capacity anomaly near T_c for the large-grained polycrystal indicates that α-U is a BCS superconductor and, hence, local moments and pair-breaking mechanisms do not play a role in its superconductivity. The known pressure enhancement of T_c is partially attributed to a density-of-states effect and partially to a reduction of the pair-weakening Coulomb repulsion as the narrow, *f*-like hybrid band broadens under pressure.

PART THREE: SmS

The heat capacity of SmS in the insulating and metallic phases has been measured between approximately 0.3 and 20 K. The entropy difference clearly shows the demagnetization of the $4f$ electrons in the metallic phase.

PART ONE: $(La,Ce)Al_2$

I. INTRODUCTION

A. Normal-Host Dilute Magnetic Alloys

In the dilute alloy systems under consideration the hosts are non-magnetic. The magnetism arises from the net spin of the crystal-field and spin-orbit split impurity ground state, which is not removed by hydridization with itinerant electron states. (Magnetism associated with singlet-ground-state systems will not be considered). Experimentally a magnetic alloy can be identified by a Curie-Weiss temperature-dependent magnetic susceptibility, χ, in an appropriate temperature interval, while a non-magnetic alloy is distinguished by a small, temperature independent χ. The entropy associated with the net spin of the impurity is usually removed in a cooperative ordering process. In a dilute magnetic alloy the usual ordering processes involve an impurity spin, $\underset{\sim}{S}$, coupling with the conduction-electron spin density, $\underset{\sim}{s}$, in the vicinity of the impurity, via the exchange Hamiltonian $-2J\ \underset{\sim}{s}\cdot\underset{\sim}{S}$, where J is the exchange interaction parameter. In the dilute limit, depending on the sign of J, spin-ordering generally proceeds either by impurity-impurity interactions or by single-impurity interactions with a spin-polarized conduction-electron sea.

In the impurity-impurity interaction region, each impurity induces in the conduction-electron sea an oscillatory spin-polarization in space. Impurities interact with each other indirectly via these spin polarizations. This interaction has been described quite successfully

by the Ruderman-Kittel-Kasuya-Yoshida (RKKY) Hamiltonian.[1] Using the RKKY interaction, Marshall[2] and others[3] have attempted to describe, within a mean-field approximation, the heat capacity anomaly associated with the removal of the impurity-spin entropy. These investigators found that the random distribution of impurities gives rise to a distribution of internal fields at the impurity site, which leads to a broad heat capacity anomaly. Although at high temperatures there is no generally valid description of the heat capacity, at low temperatures the heat capacity is characterized by a linear temperature dependence whose coefficient is independent of impurity concentration. The characteristic magnetic ordering temperature, T_M, is proportional to concentration and to J^2. Hence, T_M is independent of the sign of J. CuMn alloys with a Mn concentration of less than a few atomic percent (at.%) and greater than a few parts-per-million (ppm) is a typical system for studying impurity-impurity interactions.

The other spin-ordering process in dilute magnetic alloys involves a single-impurity interaction resulting in antiferromagnetic polarization of the conduction-electron spin density in the vicinity of the impurity. By considering the impurity-conduction electron spin-dependent contribution to the scattering processes to higher order than J^2 (the first Born approximation), Kondo,[4] in 1964, explained the resistivity minimum of certain dilute magnetic alloys. In the second Born approximation a temperature-dependent correction enters the spin-dependent contribution to the impurity scattering.[5] For $J < 0$ the corrected spin-dependent contribution to the resistivity increases logarithmically as temperature decreases. The other contributions to the resistivity decrease with

temperature, hence a resistivity minimum or "Kondo effect" appears. The corrected spin-dependent contribution to the resistivity becomes important below the Kondo temperature:

$$T_K \sim T_F \exp[-1/N(E_F)|J|], \tag{1}$$

where T_F is the Fermi temperature and $N(E_F)$ is the density of states at the Fermi energy. For $J < 0$, in the single-impurity interaction region, conduction electrons are resonantly scattered in such a way that the local impurity spin becomes compensated. The degree of compensation increases smoothly below T_K with decreasing temperature. Hence the Kondo effect gives rise to a quasibound spin-compensated state.[6]

The gradual formation of the spin-compensated state is accompanied by a broad heat capacity anomaly. Since the characteristic ordering temperature, T_K, is independent of concentration, the heat capacity shape per mole of impurity should be independent of impurity concentration. It has been experimentally verified[7] in the system CuFe that at low temperatures the heat capacity of the spin-compensated state is linear in temperature, as first calculated by Nagaoka.[8] Also, it has been verified[9] in the system CuCr that at high temperatures ($T > 0.1\ T_K$) the shape of the heat capacity of the spin-compensated state is consistent with the calculations of Bloomfield and Hamann.[10] The nature of the ground state in the single magnetic impurity problem however remains unclear.[11]

There are numerous criteria for calorimetrically distinguishing between these two spin-ordering processes in dilute magnetic alloys, even though both processes yield broad heat capacity anomalies which are linear at low temperatures. These criteria involve comparisons

of the heat capacities of alloys with different impurity concentrations. 1) At low temperatures the linear excess heat capacity coefficient in the interaction region is independent of concentration, while in the single-impurity region the coefficient per mole of impurity is independent of concentration. 2) In the interaction region the temperature of the heat capacity peak is proportional to concentration, while in the single-impurity region it is independent of concentration. 3) At high temperatures the heat capacity in the single-impurity region may be expected to decrease according to the calculations of Bloomfield and Hamann.[10]

B. Superconducting-Host Dilute Magnetic Alloys

Magnetic impurities depress the superconducting transition temperature, T_C, quite dramatically[12] compared to non-magnetic impurities. Experimental determinations of the T_C of La containing rare-earth impurities[13] indicated that impurity-conduction-electron spin-exchange scattering is responsible for this depression in T_C. By considering the affect of the spin-exchange interaction on the superconducting Hamiltonian of Bardeen, Cooper and Schreiffer[14] (BCS), in 1960 Abrikosov and Gor'kov[15] (AG) developed the theory of superconductivity in the presence of paramagnetic impurities. There are two basic assumptions in the AG theory: 1) The impurity spins are not interacting and are randomly distributed. 2) Exchange scattering need only be considered to order J^2. Hence, spin-ordering either by impurity-impurity interaction effects, or by the Kondo effect is not treated. However the AG theory provides a basis for appreciation of the problem, and also the groundwork for most subsequent developments. The AG theory indicates that

the exchange interaction, which is not time-reversal invariant, acts differently on each of the two Cooper-paired electrons (which are paired in time-reversed states). This lifts the degeneracy of the electronic states comprising each pair, causing the Cooper pairs to break and recombine for finite lifetimes, τ. Hence there is an energy broadening ($\Delta E \sim \hbar/\tau$) which fuzzes, or fills in, the superconducting energy gap. This led to the prediction of gapless superconductivity, a phenomenon which is now well-substantiated.[12] Unlike the BCS theory, the AG theory is a two-parameter theory; there is an order parameter (T_C), and an energy gap parameter. (Since the gap can go to zero before T_C does, it is the existence of pair-correlations, not the existence of a gap, which is essential to superconductivity.)

The heat capacity of an AG superconductor has many interesting features. In the low impurity concentration limit, the initial depression of T_C is:

$$\frac{T_C}{T_{C_o}} = 1 - 0.691\left(\frac{\alpha}{\alpha_{cr}}\right) \quad , \tag{2}$$

where α is the pair-breaking parameter, which is proportional to impurity concentration and inversely proportional to the Cooper-pair lifetime, τ, and α_{cr} corresponds to a T_C equal to 0 K. Also, the jump in the heat capacity, ΔC, at T_C, is reduced compared to the jump, ΔC_o, at T_{C_o}. The dimensionless parameter, c^*, the initial rate of depression of the heat capacity jump at T_C with the depression in T_C is:

$$c^* = \left.\frac{d(\Delta C/\Delta C_o)}{d(T_C/T_{C_o})}\right|_{T=T_{C_o}} \tag{3}$$

In the AG theory, c^* is 1.44, compared to unity in the BCS theory. ($c^*_{BCS} = 1$ is a statement of the law of corresponding states.) Also, due to the energy broadening associated with the Cooper-pair's finite lifetime, for even arbitrarily small impurity concentrations, the superconductor is gapless near T_C; and for concentrations greater than 91% of the critical concentration (for which T_C is 0 K), the superconductor is gapless at all temperatures. The disappearance of the gap is accompanied by the appearance of a linear term in the superconducting-state electronic heat capacity in the low-temperature limit. The magnitude[16] of the linear heat capacity coefficient, γ_S, increases smoothly from zero at 0.91 α_{cr}, to the normal-state value, γ_n, at α_{cr}.

Theoretical developments subsequent to the work of Abrikosov and Gor'kov have been reviewed by Griffin[17] and by Müller-Hartmann.[18] By relaxing the two initial assumptions of the AG theory, spin-ordering effects have been treated. Also the penetration of an external magnetic field into a type II superconductor in the mixed state, and the subsequent spin polarization it induces have been considered. These situations can be described by generalizing the pair-breaking parameter of the AG theory.

The Müller-Hartmann and Zittartz (MHZ) theory[19-25] has been developed quite extensively. In this theory for both positive and negative exchange coupling, at very low impurity concentrations, quasibound states split off in energy from the continuum, appear in the superconducting energy gap. For $J > 0$, and for $J < 0$ and $T_K \gg T_{C_o}$ or $T_K \ll T_{C_o}$, the quasibound states appear close to the gap edge. The superposition of single-impurity quasibound states leads to the

formation of an impurity band. Because of the proximity of the impurity band to the gap edge, the two tend to merge as the impurity concentration increases, resulting in a density of states which is quite similar in appearance to that of the AG theory. However, for $J < 0$ and $T_K \sim T_{C_o}$, the quasibound states can appear deep within the superconducting energy gap, leading to separated impurity bands and more than one superconducting energy gap. As the concentration of impurities increase, the gaps narrow and disappear. Hence, for $J < 0$ and $T_K \sim T_{C_o}$, the density-of-states picture is quite different than that of the AG theory. This is also reflected in the result that c^*, defined by Eq. 3, is greater than c^*_{AG}, which equals 1.44, and c^* is less than approximately 2.5. Furthermore, in the MHZ theory, for a superconductor in which there is a Kondo effect ($J < 0$), the initial rate of depression of T_C can be much greater than that predicted by AG, and the pair-breaking parameter (which in the AG theory was proportional to impurity concentration) acquires a temperature dependence. For T_K/T_{C_o} less than approximately 0.1, T_C is multi-valued for a certain range of impurity concentration. In this situation, near T_K the pair-breaking interactions are strong, and superconductivity is suppressed; however well above and below T_K pair-breaking effects are weak and superconductivity can persist.

The validity of the MHZ prediction that superconductivity will reappear well below T_K seems to be related to a particular description of the ground state of the single-impurity problem. The existence of superconductivity requires Cooper-pair correlations of the conduction-electron states, while the impurity spin-ordering requires antiferro-

magnetic spin-polarization of the conduction-electron states in the vicinity of the impurity. If superconductivity is suppressed in order to make available conduction-electron states for the impurity spin-compensation, then it is not clear that these conduction-electron states will ever again become available for Cooper-pair formation. Physically the quasibound states in the energy gap are localized in the vicinity of the impurity. In the MHZ theory these states remain localized at 0 K.

C. Experimental Evidence for a Kondo Effect in (La,Ce)Al_2

Normal-state resistivity measurements[26,27] on four (La,Ce)Al_2 samples, ranging in concentration between 1 and 5 at.% Ce substitutionally replacing La, indicate that there is a resistivity minimum at approximately 15 K which is independent of Ce concentration to within experimental uncertainty. Between approximately 2 and 6 K the magnetic contribution to the resistivity, ρ_M, is proportional to $-\ell nT$, and $\partial\rho_M/\partial\ell nT$ is proportional to concentration. The existence of the resistivity minimum and the temperature and concentration dependences of ρ_M are characteristic of a Kondo effect. The temperature dependence of ρ_M indicates that $T_K < 1$ K.

Magnetic susceptibility measurements[26,27] on four samples, ranging in Ce concentration from 0.4 to 3 at.% Ce, are in accord with a Ce $4f'$ configuration in which the $^2F_{5/2}$ Hund's rules ground term is split by the crystal field of the cubic, Laves-structure host, into a Kramer's doublet ground state approximately 100 K below a quartet. However, since the effective moment as $T\to 0$, extrapolated from above 1 K, was

approximately 30% low compared to that derived for the ground doublet of cubic Ce metal,[28] the loss of moment was attributed to the Kondo effect.

An anomalously large depression of the T_c of $LaAl_2$ (T_{c_o} = 3.3 K) doped with Ce impurities, compared to that for other rare-earth impurities, was interpreted as evidence for antiferromagnetic exchange coupling.[29] The results of this study were in agreement with the earlier work[13] on doped La. In another study, the large pressure-sensitivity of T_c of (La,Ce)Al_2, compared to (La,Gd)Al_2, in the pressure range investigated, 0 to 12 kbar, indicated that for Ce the hybridization between local and itinerant states (which causes J to be negative) could be enhanced.[30]

In 1971, soon after the MHZ prediction[22] that a Kondo effect in superconductors could lead to re-entrant normal-state behavior below T_c when $T_K < T_{c_o}$, Riblet and Winzer[31] reported the disappearance of superconductivity below a second transition temperature in (La,Ce)Al_2 below 1 K, for Ce concentrations in the vicinity of 0.8 at.%. The detailed superconducting-normal-state phase boundary (T_c vs concentration) of the system (La,Ce)Al_2 has since been determined on improved samples.[32]

Recent calorimetric measurements on four (La,Ce)Al_2 samples, with Ce concentrations between 0 and 0.5 at.%, in the temperature interval 0.5 to 4 K, have been interpreted as being consistent with the existence of a Kondo effect and superconductivity.[33,34] These measurements have been interpreted to indicate that the value of c^* is greater than c^*_{AG}, that the superconducting state is gapless at very low Ce concentrations, and that in the normal state the excess heat capacity per mole of Ce

is independent of Ce concentration. The interpretations of these measurements are not unique however. The normal-state excess heat capacity contribution, in fact, is quite similar to that of (La,Gd)Al_2, a system for which there is no evidence of a Kondo effect.[34] Since the peak in the normal-state excess heat capacity contribution in (La,Ce)Al_2 appears below 0.5 K, there was no opportunity in this study to independently verify the nature of the impurity spin-ordering process.

In the calorimetric study reported in this thesis, temperatures from 0.06 to 22 K and magnetic fields up to 38 kOe were used to explore the normal-state and superconducting-state properties of the system (La,Ce)Al_2.

II. DESCRIPTION OF THE SAMPLES

Heat capacity measurements are reported for four samples. Two of the four have previously been studied calorimetrically in the temperature interval 0.5-4.2 K at La Jolla.[33,34] Both samples exhibit superconductivity. One of these samples is nominally pure $LaAl_2$ but, according to the supplier, contained approximately 100 ppm Ce in the La starting material. The other sample contained 0.185 at.% Ce substitutionally replacing La, as determined at La Jolla from the amounts of the starting materials used in its preparation. Based on the concentration reassignment presented in Section IV.C1, this sample will henceforth be referred to as the 0.193 at.% Ce alloy.

Two new samples were prepared at La Jolla expressly for the investigation under consideration. One of these, containing 0.64 at.% Ce, lies in the narrow concentration region for which the superconducting transition temperature, T_c, is a multi-valued function of Ce concentration.[32] This sample enters the superconducting state at T_{c_1} approximately equal to 1.1 K, and upon further cooling, re-enters the normal state at T_{c_2} approximately equal to 0.25 K, T_{c_1}, and T_{c_2} are determined by a.c. mutual-inductance measurements made at La Jolla on two chips spark-cut from different parts of the arc-melted sample. The transitions are fully diamagnetic to within the approximately 10% absolute accuracy of the measurements.

The fourth sample, containing 0.906 at.% Ce, exceeds the critical concentration of Ce that destroys superconductivity at all accessible temperatures.[32] This sample was verified to be in the normal state down to approximately 0.3 K by mutual-inductance measurements. It was necessary

to anneal the sample at 800°C for one week to destroy partial superconductivity due to concentration inhomogeneities within the material.

For details of the sample preparation, the determination of the alloy compositions, and the metallurgical analyses of smaller samples prepared similarly, the reader is referred to the literature[32,33] and to C. A. Luengo's Ph.D. thesis.[34]

III. APPARATUS AND EXPERIMENTAL TECHNIQUE

A. The 0.3 to 22 K Region

1. Thermometry

The apparatus used in this temperature region employs ^{3}He refrigeration. The calorimeter contains a doped Ge resistance thermometer[35] which can give a heat capacity precision of approximately 0.1% from experiment to experiment. The Ge thermometer (Gel609) was calibrated on a recently established laboratory temperature scale designated T_η. This calibration is derived from Pt-resistance thermometry (T_{55}) between 15 and 30 K, gas thermometry between 4.2 and 20 K, the vapor-pressure of ^{4}He (T_{58}) between 4.2 and 1.1 K, the vapor-pressure of ^{3}He (T_{62}) between 3.2 and 1.1 K, and single-crystal $Ce_2Mg_3(NO_3)_{12}\cdot 12H_2O$ (CMN) magnetic thermometry below 3 K. The magnetic thermometer employs a 23 cps a.c. mutual-inductance bridge utilizing a variable reference mutual inductance[36] and lock-in detection.[37] In order to facilitate experiments in large magnetic fields, the zero-field Ge thermometer calibration was preserved by positioning the thermometer in a low-field region of the apparatus and inside a mumetal[38] shield.

2. The Heater

The calorimeter also contains a 7 KΩ heater non-inductively wound from 14 feet of 0.0009 inch diameter Pt-9%W wire.[39] The heater is well-suited for low temperature calorimetry because it has a low heat capacity,[40] and low magnetic-field and temperature coefficients

of electrical resistance in the temperature region of interest. Power generated in the matched heater leads is automatically accounted for by connecting one potential lead to a current lead at the calorimeter, and the other potential lead beyond the thermal isolation section of the other current lead.[41] The heater is actuated by a mechanical relay, with Hg wetted contacts, which is powered by a 10.8 volt Hg cell. Photocouplers totally isolate the heater circuit from the associated heater-timing circuit and all other circuits. Typical heating times range from 4 to 16 seconds--these times are known to an accuracy of 0.1 millisecond.

3. Thermal Contact to the Calorimeter

The calorimeter is rigidly suspended in a vacuum space in the cryostat using fine nylon monofilament. At low temperatures thermal contact between the calorimeter and the refrigerant is established via mechanical heat switches. In initially cooling the apparatus from room-temperature, approximately 500 microns of N_2 exchange gas is utilized. At liquid -N_2 temperature the exchange gas is evacuated and replaced with approximately 500 microns of H_2 exchange gas, which is evaculated at approximately 12 K. The H_2 gas is especially useful since it facilitates the cooling of parts of the mechanical heat switch and electrical lead system which are not in good thermal contact with the refrigerant. Care is taken to eliminate H_2 from adhering to the calorimeter surface.

4. The Sample Solenoid

Experiments performed in magnetic fields utilize a superconducting solenoid of 38 kOe maximum field, operated in the persistent mode. The solenoid wire is a Cu-clad, oxide insulated, single-core NbTi alloy. The calibration of the solenoid is based on an analyses of its turn density and geometry. The field is homogeneous to 0.1% over the volume of a sample. The approximately 0.5% accuracy to which the field is known is limited by the series shunt of the power supply.[42] During an experiment the field was generally monitored by a rotating--coil gaussmeter or Hall probe located outside the cryostat. At the end of an experiment the field could be checked by the solenoid's discharge characteristics.

For details of the calorimeter design and solenoid specifications the reader is referred to B. B. Triplett's Ph. D. thesis.[43]

5. Sample Mounting

The calorimeter is fabricated predominantly of Cu, and it terminates in a threaded bobbin to accept tapped samples. Since the (La,Ce)Al_2 samples were not suitable for machining, a silver adapter was used to mount the samples to the calorimeter. The tapped Ag adapter contains a Ag foil section that enclosed the sample. GE7031 varnish[44] was used to bond the sample to the Ag foil and to enhance the thermal coupling of the sample to the calorimeter.

6. The Heat Capacity of a Sample

The heat capacity C of a sample per mole of $La_{1-x}Ce_xAl_2$, is calculated from the following equation:

$$C = [(C_{Total} - C_{MT} - C_{Ag} - C_{GE7031})/n] \qquad (4)$$

where n is the number of moles, C_{Total} is the total heat capacity measured, C_{MT} is the heat capacity of the empty Cu calorimeter, C_{Ag} is the heat capacity of the Ag adapter, and C_{GE7031} is the heat capacity of the varnish used to bond the sample to the Ag adapter. C_{Total} is obtained by the heat pulse technique. The width $(T_{final} - T_{initial})$ of a measured heat capacity point is approximately T/10. A curvature correction is applied to C_{Total} to correct for the finite width of a point. This correction is generally 0.1% or less. Each contribution subtracted from C_{Total} will now be discussed separately.

7. The Heat Capacity of the Addenda

The heat capacity of the empty calorimeter is

$$C_{MT} = [A(H)T^{-2} + \sum_{i=1}^{6} B_i T^{b_i}] \cdot [1 + \Delta(T,H)] \quad , \qquad (5)$$

where the b_i = 1,2,3,5,7 and 9. The $\Delta(T,H)$-values are interpolated from smooth curves drawn through the fractional differences between the measured heat capacity and that calculated from least-squares fitting the data to the expression appearing in the first bracketed term to the right in Eq. (5). The Δ-values make corrections to the calculated equation of the order of 0.1%. The coefficient A(H) in Eq. (5) predominantly reflects the magnetic-field sensitivity of the nuclear heat capacity of ^{63}Cu and ^{65}Cu. The field dependence of the

Δ-values predominantly reflect the weak magnetism of the epoxy[45] (Stycast 2850GT and catalyst no.9) sparingly used to thermally anchor the electrical lead system to the calorimeter. This epoxy is reported to have a temperature-dependent paramagnetic susceptibility in the liquid-He temperature region.[46] The only fields for which experimental determinations of A(H) and Δ(H,T) can be applied to the data under consideration are 0 and 38 kOe. For the low-field experiments, the zero-field A(H) and Δ-values were retained. For the 20 kOe experiments all Δ-values were set equal to zero, and A(H) was estimated assuming $A(H) = \alpha H^2 + \beta$, where α and β are constants. The functional dependence of A(H) is consistent with experimental data for the empty calorimeter in 9 and 27.9 kOe.

C_{Ag} was calculated from

$$C_{Ag} = [\gamma_o T + \sum_{i=1}^{4} B_{2i+1} T^{2i+1}] \cdot X \qquad (6)$$

with the coefficients B_{2i+1} determined by fitting to Martin's 3-to-30 K data[47] and using Martin's determination of γ_o of 0.646 mJ/K^2 mole. For X, the number of moles of Ag, the weight of the adapter was utilized, ignoring corrections due to the milligram-quantity of hard-solder (a 50% Ag brazing alloy) used to join the tapped part of the adapter to the foil section. The adapter was fabricated from "as-received" 6-9's Cominco[48] Ag. The fractional differences to the fit were not used to construct a Δ-table to improve the determination of C_{Ag}. These Δ-values probably would be determined to a significant degree by

Martin's temperature scale, which is no doubt slightly different from that used here.

The equation:

$$C_{GE7031} = [\sum_{i=1}^{8} A_i T^i] \cdot [1 + \Delta(T)] \cdot Y \qquad (7)$$

was obtained by least-squares fitting to a) the experimental data by Cude and Finegold[49] for $4 \leq T \leq 18$ K, b) the smoothed data by Hessels[50] for $2 \leq T \leq 5$ K and $20 \leq T \leq 35$ K, and c) the smoothed data by Phillips[51] for $1.5 \leq T \leq 4$ K, reduced in magnitude by approximately 12% to join the data by the other investigators in the temperature region of overlap. The large amplitude ($|\Delta| \lesssim 0.1$) and systematic variations of the fractional differences to the fit required the inclusion of a Δ-table to adequately represent C_{GE7031}. The number of grams of varnish used, y, was generally between 0.02 and 0.05 g. The varnish was thinned by mixing 2 parts of it to 1 part toluene and 1 part methanol, and it was cured at room temperature. The differences between the reported heat capacities of the varnish in the literature probably arise from slight variations in the thinning and curing processes.

B. The 0.06 to 1 K Region

1. Refrigeration

A new apparatus was used in this temperature region, which employs magnetic cooling. The apparatus is similar to previous systems used in this laboratory except that it makes heat capacity experiments in large magnetic fields feasible. This feature was accomplished by physically locating the sample solenoid far from the cooling salt.

The cooling salt, approximately one-half mole of chrome potassium alum, $KCr(SO_4)_2 \cdot 12H_2O$, is adiabatically demagnetized from an initial temperature of approximately 1.2 K and an initial field of approximately 12 kOe. The field is produced either by a superconducting solenoid, or by a conventional electromagnet mounted on a non-magnetic track. (The track enables the electromagnet to be physically removed from the area of the cryostat in order to reduce the remnant field to a background level.) The cooling salt consists of an irregular distribution of crushed single crystals coated with Apiezon N grease[52] and mixed with no. 40 gauge Cu wires. The mixture was packed into a leak-tight, low-lead brass (Alloy 260) can containing an array of 0.005 inch Cu fins oriented to minimize eddy-current heating during demagnetization. The surface area of metal-to-salt contact inside the can is approximately 900 cm^3.

The sample solenoid and the electromagnet used in refrigeration cannot simultaneously be fully charged because of the forces between them. However, if the sample solenoid is charged after completion of the adiabatic demagnetization process, the eddy-current heating generated puts a large load on the accessible cooling capacity of the chrome potassium alum salt. This is due to a rapidly increasing internal thermal time constant of the cooling salt below 0.1 K. The procedure followed to simultaneously achieve high field and low temperature conditions involves an interrupted demagnetization. At approximately 0.15 K the cooling process is halted--essentially all of the cooling capacity of the salt is accessible--the field is applied

to the sample, thermal equilibration between the sample and coolant reestablished, and then the demagnetization of the coolant is slowly completed. Using this procedure samples have been cooled to the 50 mK region in fields up to 38 kOe in this apparatus.

2. The Calorimeter

The calorimeter is quite similar in appearance to the calorimeter discussed in the previous section. However, the calorimeter is fabricated predominantly of 5-9's pure Cominco[48] Ag. The heater and electrical lead system is thermally anchored to the calorimeter with a non-magnetic epoxy (equal parts Epon 828 and Versamid 140).[53]

3. The Heat Switch

Thermal coupling between the calorimeter and the coolant is controlled below 1 K using a superconducting Pb heat switch. The functioning of the switch involves the orders of magnitude difference in the electronic thermal conductivity of pure elemental superconductors well below T_c. At low enough temperatures the lattice contribution to the thermal conductivity becomes small and the electronic component can be driven from a low value in the superconducting state to a high value in the normal state by application of a magnetic field (greater than 800 Oe in the case of Pb) to suppress superconductivity. The apparatus utilizes a Pb wire of appropriate dimensions to provide excellent thermal isolation in the superconducting state below approximately 0.6 K. Above 0.6 K the coolant and calorimeter are kept at similar temperatures to minimize the heat leak across the Pb switch. In this manner reasonable heat capacity data have been obtained on occasion up to 2 K.

The switch is controlled by a superconducting Nb solenoid compensated to cancel the dipolar term in the stray field.[54] This solenoid is mounted in the vacuum space along with the calorimeter and cooling salt, but it is thermally anchored to the ^{4}He bath.

4. The Sample Solenoid

As in the ^{3}He-cooled apparatus, experiments performed in magnetic fields utilize a superconducting solenoid operated in the persistent mode. The solenoid was wound on an epoxy-fiberglass former.[55] The organically insulated, 0.009 inch diameter solenoid wire[56] contains 400 twisted 10 micron diameter filaments of NbTi alloy embedded in Cu. The 0.011 inch diameter wire used in the solenoid's persistent-mode switch contains 22 twisted strands of NbTi alloy embedded in a low thermal conductivity CuNi alloy.[57] The joint between the solenoid wire and the persistent-mode switch wire was made by In soldering 6 inch lengths of the wires, and by pressure-welding the exposed NbTi filaments to the strands.[58] Spot-welding was not attempted because of the fragility of the filaments. The solenoid was characterized by low remnant fields, fast charge rates, and a homogeneity of a few tenths of a percent over the volume of a sample. At 4.2 K the solenoid consistently quenched at 15.8 kOe, and in superfluid ^{4}He at 21.6 kOe (at a current of 54 Amps). The solenoid was charged and discharged via two electrical leads of insulated no. 18 gauge Cu wire, utilizing efficient ^{4}He gas-cooling provided by the boil-off of the 1 K ^{4}He bath. The calibration and field profile of this solenoid also is based on calculations.

5. Thermometry

The Ge resistance thermometer (Ge2345) was calibrated on the laboratory scale T_η as described in the previous section. In this case the calibration was extended using CMN magnetic thermometry down to 0.055 K, and Pt-resistance thermometry up to 80 K. The calibration data were processed in three separate temperature intervals. One of these intervals, 0.055 to 5 K, encompassed the entire calorimetric temperature range of interest. During an in-field experiment the thermometer experienced a maximum field of approximately 150 Oe. Based on the magnetoresistance of similar Ge thermometers, this field does not significantly affect the zero-field calibration.

6. The Heat Capacity of Pure Copper

The functioning of the apparatus was tested by measuring the heat capacity of a vacuum-melted, 6-9's pure American Smelting and Refining Company (ASARCO) Cu sample. This same sample had been measured previously several times in the ^{3}He-cooled apparatus described earlier. On the laboratory temperature scale T_η the leading terms of the Cu heat capacity are characterized by $\gamma_o = 0.695$ mJ/K^2 mole and by a Debye temperature, θ_o, of 348.7 K. In the temperature region of overlap between the two calorimeters, 0.3 to 1 K, the fractional differences to the same Cu fit were always in agreement to within a few tenths of a percent.

7. The Heat Capacity of the Addenda

For the data obtained in the magnetic-cooling apparatus, the molar heat capacity of a sample is again defined by Eq. (4). However,

the empty Ag calorimeter is simply characterized by $C_{MT} = \gamma_o T + B_3 T^3$; γ_o and B_3 were determined experimentally in 0, 2 and 20 kOe. The heat capacity of this calorimeter is magnetic-field independent to approximately 0.1 K to within ± 2% in these fields. This field-independence is attributable to the small nuclear magnetic moments of Ag, and to the use of the non-magnetic epoxy. A low-temperature, field-independent heat capacity anomaly, however, appears in this calorimeter and in another Ag calorimeter used by Triplett.[43] This anomaly contributes approximately 1% at 0.3% and approximately 4% at 0.1 K to C_{MT}. It is possible that this anomaly is a property of the Ag. Heat capacity measurements for Ag appear in the literature[59] only for temperatures above 0.4 K, but it is well-known that dissolved H_2 produces a low-temperature heat capacity anomaly in Cu. The Ag calorimeter anomaly was not corrected for, since it is unclear how to extrapolate it below 0.1 K. Fortunately, at these temperatures the sample heat capacity always dominates C_{Total}, making it unnecessary to precisely characterize C_{MT}.

The heat capacity of the Ag adapter is represented by $C_{Ag} = (\gamma_o T + B_3 T^3 + B_5 T^5) \cdot X$, using the leading terms in Eq. (6), the fit to Martin's data, to define the coefficients.

The heat capacity of the varnish was represented by Phillips' determination[51] of $C_{GE7031} = (B_3 T^3 + B_5 T^5) \cdot Y$, because the expression used at higher temperatures, Eq. (7), is not suitable for low temperature extrapolation. A discontinuity generally less than 0.03%

below 1 K results from applying the different characterizations of C_{GE7031} to the data in the two calorimeters. No attempt has been made to explore the existence of a linear contribution to C_{GE7031} in this study, although in recent years an anomalous linear term in the low-temperature heat capacity of many amorphous substances has been experimentally detected.[60-63] The nature of the amorphous state[64] or perhaps the lattice dynamics of materials rich in voids[65] account for the appearance of the linear heat capacity contribution. In any case, it is estimated from the previous reports that any linear heat capacity coefficient would be of the order of 1 $\mu J/K^2 g$--a value too small to be important in the data analysis.

IV. RESULTS AND DATA ANALYSIS

A. Summary of the $(La,Ce)Al_2$ Measurements

A total of 26 heat capacity experiments are reported for the four samples:

Experiment	Sample (at.% Ce)	Field (kOe)	Temperature Interval (K)
1	0.0	0	0.4-22
2	0.0	1	0.4-18
3	0.0	3	0.4-7
4	0.193	0	0.1-1.4
5	0.193	0	0.09-0.4
6	0.193	2	0.4-22
7	0.193	20	0.4-21
8	0.193	20	0.065-0.4
9	0.193	38	0.3-21
10	0.64	0	0.065-0.4
11	0.64	0	0.3-21
12	0.64	0.5	0.1-0.5
13	0.64	0.5	0.36-7
14	0.64	2	0.06-2
15	0.64	20	0.08-1
16	0.64	20	0.5-13
17	0.64	38	0.4-21
18	0.906	0	0.07-0.6
19	0.906	0	0.3-23
20	0.906	0.5	0.1-0.6
21	0.906	0.5	0.3-13
22	0.906	2	0.07-0.6
23	0.906	2	0.4-13
24	0.906	20	0.07-0.6
25	0.906	20	0.5-13
26	0.906	38	0.4-20

The high temperature data for all four samples in zero field are shown in Fig. 1 as C/T^3 vs T. Above 14 K the differences between the heat capacities of the various samples are small (less than 2.5%) and proportional to T^3. These differences do not show a systematic trend with Ce concentration, hence they do not represent a variation in C with alloying. They are probably due to an incorrect characterization of the heat capacity of the varnish used to bond a sample to the Ag calorimeter adapter. In the 14 to 20 K region the heat capacity of the GE7031 varnish has a T^3 dependence to within ± 20%, and the varnish comprises approximately 1% of the total measured heat capacity. Since in this same temperature interval the sample comprises approximately 20% of the total measured heat capacity, scaling the varnish contribution for each alloy < 30% brings the alloy data into coincidence with the $LaAl_2$ data to within experimental scatter. In Section III-A it was mentioned that a scaling factor of a similar order of magnitude was necessary to join the different determinations of the heat capacity of the GE7031 varnish reported in the literature. The irreproducibility of the varnish heat capacity is probably due to variations in the details of the thinning and curing processes. All alloy data taken in the ^{3}He-cooled calorimeter have been adjusted to bring their C/T^3 curves of Fig. 1 into coincidence with that of the $LaAl_2$. This adjustment obscures any real differences in C_L, the lattice heat capacity, with alloying. However, such an affect, if it exists at all, must be small. No adjustments have been applied to the $LaAl_2$ data.

B. $LaAl_2$

The next step of the data analysis is to characterize the host heat capacity in order to define the excess, or impurity spin contribution to the heat capacity of the alloys. Twenty-seven data points of the nominally pure $LaAl_2$ in zero field have been least-squares fitted between 4 and 22 K to the expression:

$$C_{host} = \gamma_n T + \sum_{i=1}^{4} B_{2i+1} T^{2i+1} \qquad (8)$$

where C_{host} is in mJ/K mole $LaAl_2$, and

$$\gamma_n = 9.6517349 \ ,$$
$$B_3 = 7.99946 \times 10^{-2} \ ,$$
$$B_5 = 6.38357 \times 10^{-4} \ ,$$
$$B_7 = 3.11439 \times 10^{-8} \ ,$$
and $$B_9 = -1.1086 \times 10^{-9} \ ,$$

The subscript in γ_n denotes that it is the normal-state γ-value. The four-term summation represents the lattice heat capacity, C_L. The r.m.s. deviation of the fit is 0.6%. A plot of the fractional differences to the fit as a function of temperature yields a fairly random scattering of points about zero. There is not enough definition in the systematic variations of the residuals to construct a Δ-table in order to further improve the characterization of C_{host}. The B_3-term (per mole of $LaAl_2$) corresponds to a Debye characteristic temperature, θ_o, of 290 K. The

leading terms, γ_n and B_3, obtained graphically from C/T vs T^2 plots are consistent with the computer fit values for the sample in zero field (above T_c), and in 1 and 3 KOe in appropriate temperature ranges.

For the in-field experiments, Eq. (8) is modified to include a calculated term, C_N, proportional to H^2/T^2 for the nuclear heat capacity of the host in the applied field. Implicit in this approach is the assumption that Knight shift corrections are small. It seems reasonable to assume that Knight shifts averaged over the volume of the sample are $\lesssim$ 1% based on studies of other dilute alloy systems.

The $LaAl_2$ data below 4 K appear in Fig. 2 plotted as C_E/T vs T, where C_E, the electronic heat capacity is $C-C_L-C_N$. The straight horizontal line represents the γ_n-value determined from the fit. In zero field in the vicinity of T_c the heat capacity points have a width, T_f-T_i, of approximately T/30. There is only one point for which $T_i < T_c < T_f$. This point is used to define T_c = 3.307 K from the equation:

$$\int_{T_i}^{T_f} C_E dT = \int_{T_i}^{T_c} C_{Es}(T)dT + \int_{T_c}^{T_f} C_{En}(T)dT \qquad (9)$$

where C_E is the value of the electronic heat capacity of the point, C_{En} is the normal-state electronic heat capacity $\gamma_n T$, and C_{Es}, the superconducting state heat capacity, is equal to αT^{β} near T_c, with α and β determined from a line drawn through a log C_{Es} vs log T plot. The jump in C_E at T_c is 95% of a BCS heat capacity jump[66] of 1.43 $\gamma_n T_c$.

Both the normal state and the superconducting state show evidence of impurity effects. It is known that the La starting material contained on the order of 100 ppm Ce impurity. The rise in C/T below 1 K in the 3 kOe experiment and the deviations from the BCS reference curve[67] in the zero-field experiment, both shown in Fig. 2, will be related to the presence of Ce in Section V, after the results of the alloy experiments have been presented. Smoothly extrapolating C_{Es}/T to zero (or near zero) at T = 0 K enables the entropy to be determined at T_c and compared with the normal-state electronic entropy, $\gamma_n T_c$. If this method of extrapolation is correct the superconducting-state and the normal-state entropies will be equal, since there is no latent heat at T_c. The superconducting-state entropy at T_c,

$$S_{Es}(T_c) = \int_o^{T_c} \frac{C_{Es}(T)}{T}\, dT \qquad (10)$$

is approximately 5% lower than $S_{En} = \gamma_n T_c$. Hence C_{Es}/T cannot be extrapolated to T = 0 K in the usual manner. This property of the superconducting state is related to the presence of Ce impurities and it will be discussed further in Section V.

C. Normal-State Alloy Data

1. High Fields

The excess, or impurity spin heat capacities of the alloys in the normal state were calculated per mole of Ce from:

$$\Delta C/c = (C - C_{host})/c \qquad (11)$$

where c is the molefraction of Ce substitutionally replacing La. $\Delta C/c$ vs T (on a logarithmic scale) is plotted for the 0.906 at.% Ce sample in Fig. 3. Smooth curves a and b were drawn to represent the 38 and 20 kOe data respectively. (Curve b was drawn systematically above the data between about 2 and 3 K and below the data between about 3 and 7 K, in order to provide a reasonable high-temperature extrapolation of the data without underestimating the entropy associated with the impurity spin ordering in 20 kOe.) The full length of the vertical bars appearing at the higher temperatures represent the affect of a 1% error in the total measured heat capacity. Curves a and b of Fig. 3 are reproduced in Fig. 4 which illustrates the data for the 0.64 at.% Ce sample. In each of these fields the agreement between the data for the two alloys is excellent. Extrapolating the high-temperature sides of the curves to zero smoothly, enables the impurity spin entropies to be determined by graphical integration. The entropy values in both fields are (1.01) Rln2. This entropy-value confirms the existence of a crystal-field ground state of effective spin 1/2. It also confirms that Eq. (11) correctly separates out the impurity-spin heat capacity contribution from C. Since the lattice contributions were effectively equalized, this indicates that the γ-values of the alloys are not enhanced above γ_n, the host γ-value.

The high-field $\Delta C/c$ data of the two more concentrated samples are in excellent agreement. However, the corresponding data of the dilute sample, in comparison, was found to be systematically high when using for its concentration the La Jolla value, 0.185 at.% Ce,

based on the amounts of starting materials used in the alloy's preparation. The concentration of the dilute sample was then reassigned the value 0.193 at.% Ce to bring the high-field data of all three alloys into coincidence within experimental error. This is illustrated in Fig. 5 by the good agreement between the 38 and 20 kOe data with curves a and b of Figs. 3 and 4. Taking into account the Ce impurity in the La starting material, estimated by the supplier to be on the order of 100 ppm or 0.01 at.% Ce, the concentration determined by scaling the high-field heat capacity data agrees remarkably well with the concentration determined from the actual amount of Ce used in preparing the alloy. Furthermore, recognition of the additional 0.01 at.% Ce in the more concentrated samples could account for the impurity-spin entropy being 1% high compared to Rln2.

2. Low Fields

Figure 3 also illustrates the excess heat capacity per mole of Ce for the 0.906 at.% Ce alloy in 0, 0.5 and 2 kOe. The broad heat capacity anomaly characteristic of dilute magnetic alloys is apparent. For all three fields $\Delta C/c$ peaks at approximately 0.14 K, although in 2 kOe the field has enhanced the peak height significantly. Curve c of Fig. 3 represents the 2 kOe data. To facilitate comparison of the 2 kOe experiments, curve c of Fig. 3 is reproduced in Figs. 4 and 5. To a good approximation $\Delta C/c$ is independent of Ce concentration, showing that these alloys are exhibiting single-impurity behavior. The $\Delta C/c$ comparison is made in 2 kOe in order to suppress superconductivity and therefore to facilitate an unambiguous host heat capacity

characterization. Fortunately 2 kOe does not alter the temperature at which $\Delta C/c$ peaks in zero-field, as was shown in Fig. 3.

Curve d of Fig. 3 fits the experimental data for the system CuCr in the spin-compensated state.[9,43] This curve is shifted in temperature to coincide with the (La,Ce)Al_2 $\Delta C/c$ peak, and it is scaled down in height by a factor of 2 since CuCr is a spin 3/2 system (Rln2 = 1/2 Rln4). Curve d originally derives from calculations by Bloomfield and Hamann of the heat capacity of dilute magnetic alloys which exhibit a Kondo effect.[10] The agreement between the zero-field data in Fig. 3 and curve d provides calorimetric confirmation of the existence of a Kondo effect in the (La,Ce)Al_2 system.

D. Superconducting-State Alloy Data

In zero field the 0.64 at.% Ce alloy is in the superconducting state between T_{C_1} and T_{C_2}. The mutual-inductance determinations of these transitions are $T_{C_1} = 1.1 \pm 0.15$ K and $T_{C_2} = 0.25 \pm 0.10$ K, where the widths are taken to be the 10 to 90% spreads of the normalized transition signal. The zero-field data appears in Fig. 4, but Eq. (11), the definition of $\Delta C/c$, is no longer valid since C_{host} cannot be represented by Eq. (8) below T_{C_1}. The zero-field data does however indicate the similarity of the superconducting-state heat capacity to that of the normal state. In fact the broadened jump in the heat capacity that appears at the onset of the calorimetric transition at approximately 1.25 K is barely detectable. In the vicinity of T_{C_2} the data are smooth with no evidence of even a smeared-out anomaly.

In 0.5 kOe the smeared-out, zero-field jump in the heat capacity at T_{c_1} is suppressed. Below T_{c_1} the 0.5 kOe data are systematically above the zero-field data. This behavior is expected since the field 1) suppresses superconductivity, and 2) enhances the excess heat capacity of the Ce impurity in this temperature region. Both effects are small but apparent.

The zero-field data for the 0.193 at.% Ce alloy is plotted in Fig. 6 as $(C-C_L)/T$ vs T. The condition $T_i < T_c < T_f$ is satisfied for only one point. Using this one point and Eq. (9), $T_c = 2.83$ K is obtained. Again $C_{Es}(T)$ near T_c was obtained from a log C_{Es} vs log T plot. In using this empirical characterization of T_c it should be appreciated that the superconducting state should actually be characterized by a distribution of T_c-values produced by the Ce concentration inhomogeneity within the alloy. Although a reasonable distribution of T_c-values can be chosen, no quantitatively reliable representation of $C_{Es}(T)$ exists for this particular alloy system.

In Fig. 6, the horizontal line represents the γ_n-value of Eq. (8). The dashed curve above this line represents the combined contributions of the normal-state electronic plus impurity-spin heat capacity divided by temperature. The impurity-spin contribution was obtained by scaling the zero-field ΔC for the 0.906 at.% Ce alloy to the concentration of the dilute alloy. The dot-dashed curve represents the impurity spin contribution alone. The experimental data in Fig. 6 contains the combined contributions of the superconducting-state electronic plus impurity-spin heat capacity. Comparing the dot-dashed curve to the experimental data, it is clear that below 0.55 K the combined

superconducting-state heat capacity of the conduction-electronic and impurity-spin system is less than the normal-state heat capacity of the impurity-spin system alone. Hence the characteristic ordering temperature of the impurity-spin system is substantially depressed in the superconducting host for this alloy.

The difference between the normal-state entropy and the superconducting-state entropy can be determined between the lowest temperature (T_ℓ), 0.08 K, for which there are experimental data, and T_c. Between 0 K and T_c the difference in the conduction-electronic entropy between the normal and superconducting state must be zero, and between T_ℓ and T_c the normal-state conduction-electronic entropy must be less than that of the superconducting state. However, graphical integration of the smoothed zero-field data, and of the dashed curve of Fig. 6 indicates that between T_ℓ and T_c the combined normal-state conduction-electronic and impurity-spin entropy is greater than the combined superconducting-state conduction-electronic and impurity-spin entropy. This difference between the two entropy determinations, approximately 4.2 mJ/K mole, provides an indication of the extent to which the formation of the spin-compensated state has been suppressed in the superconducting host compared to the normal host for this alloy. Estimates of T_K in the superconducting (and normal) host will be discussed in Section V.

V. DISCUSSION

A. $LaAl_2$

1. Normal-State Data Comparisons

The normal-state electronic heat capacity coefficient of the "pure" $LaAl_2$ of 9.65 mJ/K^2 mole agrees with the value 9.55 mJ/K^2 mole determined earlier by Luengo et al. for this same sample.[33] The approximately 1 % difference in the two γ-value determinations probably represent slight differences in the temperature scales of the two laboratories and small systematic errors in the data analyses--similar differences are typical for inter-laboratory comparisons of calorimetric standards.[3]

The agreement between the Debye characteristic temperature (θ_o) determinations, however, is not satisfactory. The θ_o found in this study is 290 K. Luengo et al. obtained a θ_o-value of 376 K by assuming C_L is equal to B_3T^3 throughout the range of their measurements, which extend to 4.2 K. There are numerous problems associated with attempts to characterize θ_o uniquely. In the low temperature limit the temperature dependence of the heat capacity of a normal metal can be represented by a linear plus a cubic term, for C_E and C_L respectively, assuming that magnetic and nuclear contributions are negligible. However, for a metal with a large electronic heat capacity, as in this case, the lattice contribution becomes a small fraction of the sample heat capacity at low temperatures and hence cannot be precisely determined. In these cases small systematic errors also can strongly

affect C_L and hence θ_o. At higher temperatures where C_L becomes significant compared to C_E, C_L does not necessarily have a simple cubic temperature dependence. The method of least-squares fitting higher temperature data to a power series expansion of C_L to obtain θ_o from the B_3T^3 term is generally quite reliable (however it might be sensitive to unknown shortcomings of the laboratory temperature scale compared to the thermodynamic temperature scale). In this study the C_L of $LaAl_2$ at 4 K was approximately 13% of the heat capacity of the sample, or approximately 4% of the total heat capacity measured, and the B_3T^3 term was approximately 88% of C_L. Hungsberg and Gschneidner[68] measured the heat capacity of $LaAl_2$ of similar purity to that of this study, based on their T_c value of 3.29±0.03 K. Above T_c they obtained (per mole of $LaAl_2$) a γ_n of 11 mJ/K^2 mole and θ_o of 244 K. They indicated that using a T^5 term in addition to the T^3 term to represent C_L increased θ_o on the order of 10%. Hence their data can be interpreted to yield a θ_o consistent with that of this study; however the γ_n-values differ systematically. Machado da Silva et al.[69] measured the heat capacity of $LaAl_2$ between 0.2 and 4 K. They obtained a T_c of 2.75 K, and in the normal state γ_n was 12.1 in mJ units and θ_o was 195 K (per mole $LaAl_2$). Clearly the low value of T_c indicates that impurity effects are significant in this sample, hence the determination of the normal-state properties are in doubt. In cases such as that for $LaAl_2$ an independent determination of θ_o from elastic-constants measurements often is quite useful. Until such data become available, given the excellent agreement between

the two independent C_E determinations of the sample used in this thesis research, the good precision of the data, and the extended temperature range of the measurements, the 290 K value of θ_o probably represents the best value to date.

2. Normal-State Evidence for Ce Impurities

At the lowest temperatures in Fig. 2 the shape of the 1 kOe heat capacity data suggests that in this field there might be a broadened, partial superconducting transition. In 3 kOe at the lowest temperatures there is an anomalous increase in C_E/T that appears not to be associated with superconductivity. Comparing the 3 kOe heat capacity in excess of $\gamma_n T$ at 0.5 K in Fig. 2 to the 2 kOe $\Delta C/c$ for the alloys, a concentration of approximately 160 ppm Ce impurity is required to explain the anomaly. This is in reasonable agreement with the 100 ppm Ce impurity concentration estimated by the La supplier.

3. Superconducting-State Behavior

In Fig. 2 the superconducting-state data was compared with the BCS representation of C_{Es}. It is plausible that at T_c the reduction in the heat capacity jump compared to the BCS jump can be explained qualitatively within the theory of dirty superconductors.[70] Non-magnetic impurities (i.e., dirt) act as potential-scattering centers which alter the nature of the pairing that takes place in the superconducting state in such a way as to eliminate anisotropy (due to the existence of preferred directions in momentum space relative to the crystal axes) from having an advantageous affect on pair formation. Based on a BCS-like model proposed by Markowitz and Kadanoff[71] the effects of the

elimination of anisotropy upon the heat capacity jump have been calculated by Clemm[72] and expressed in terms of the mean squared anisotropy $\langle a^2 \rangle$, an angular average of a function which describes the anisotropy of the superconducting energy gap. The reduction in the heat capacity jump at T_c relative to the BCS jump is consistent with an $\langle a^2 \rangle$ -value of 0.02, which is a typical value for a weak-coupled superconductor. However, at the lower temperatures to which the experimental data extend no reasonable $\langle a^2 \rangle$ -value can explain the deviation of C_{Es} from the (isotropic) BCS curve. Therefore it is concluded that the shape of the $LaAl_2$ superconducting-state heat capacity cannot entirely be explained within a BCS framework.

It appears that magnetic scattering processes are necessary to explain the shape of C_{Es}. Taking this point of view and assuming Ce impurities are solely responsible for the reduction in the heat capacity jump at T_c, it would require 290 ppm Ce to produce the total effect. (This estimate is based on the experimental determinations of the initial (dT_c/dc) of - 2.56 K per at.% Ce, and c^* of 2.2, appearing in Refs. 32 and 33, respectively.) It is gratifying that this independent estimate of the Ce impurity concentration of the $LaAl_2$ sample is of the same order of magnitude as the previous estimates. This new estimate differs, however, by factors of roughly 2 and 3 from that based on the 3 kOe normal-state data, and that of the La supplier, respectively. The behavior of C_{Es} near T_c can be reasonably described assuming approximately 160 ppm Ce impurity and a gap anisotropy, $\langle a^2 \rangle$, of approximately 0.01.

In Section IVB an approximately 5% entropy discrepancy in the $LaAl_2$ sample between $S_{Es}(T_c)$ and $S_{En}(T_c)$ was taken to indicate that C_{Es}/T cannot be extrapolated to zero (or near zero) in the usual manner. It has since been demonstrated in the alloys that a Kondo effect is responsible for the Ce impurity spin ordering that quite dramatically affects the superconducting properties of the system. It also has been demonstrated, using a variety of approaches, that there is clearly a small concentration of Ce impurity in the nominally pure $LaAl_2$ sample. The apparent entropy discrepancy can be removed (as it must according to the third law of thermodynamics) if C_{Es}/T increases below the experimental temperature region explored. Such behavior viewed within an electronic-density-of-states framework indicates that there are states located deep within the energy gap of the pure superconductor. The existence of quasibound states within the superconducting energy gap has been predicted theoretically by a number of independent investigators[73] for superconductors exhibiting a Kondo effect with $T_K \sim T_{C_o}$. Physically these states may be viewed as broken Cooper-pair states, trapped around Ce impurities, which provide the antiferromagnetic spin-pairing by which the impurities order and are spin-compensated. This behavior provides yet another dramatic demonstration of the Kondo effect in superconductors.

B. Normal-State Alloy Data

1. Data Comparisons

Luengo et al. measured the heat capacity of the 0.193 at.% Ce alloy and that of two other alloys not studied here.[33] They concluded from their $(C-C_L)/T$ vs T^2 plots that there is a strong enhancement of γ_n for these alloys which scales with Ce concentration, in addition to the low-temperature anomaly associated with the formation of the spin-compensated state. Although in the current study, plots of C/T vs T^2 for the alloys over limited temperature ranges appear to yield enhancements in the linear heat capacity contribution, the effect depends on the temperature range under consideration since the plots exhibit significant curvature at all temperatures. (Low-temperature plots of C/T vs T^2 reliably define C_E and C_L only when there are no magnetic and nuclear contributions to the heat capacity.) The excellent agreement of the experimentally determined excess entropies in high fields with that expected for an effective spin 1/2 system indicates that C_E of the alloys are identical, within experimental uncertainty, to that of $LaAl_2$. Furthermore, without assuming enhancements of the γ-values of the alloys, the 0 and 0.5 kOe excess heat capacities of the 0.64 and 0.906 at.% Ce alloys are quantitatively consistent with the single-impurity behavior of the well-characterized experimental system CuCr and the theoretical calculations of Bloomfield and Hamann[9,10] up to a temperature at least twenty-times greater than the temperature of the excess heat capacity

peak (T_p). (Even above approximately 20 T_p, or 3 K, the systematic deviations of the low-field $\Delta C/c$ data of Fig. 3 and Fig. 4 compared to the curves labelled d, are always less than 1% of the total heat capacity measured and within the presumed accuracy of the measurements.) Hence it is clear that the apparent γ-value enhancements reported by Luengo et al. actually represent the high-temperature contribution of the broad heat capacity anomaly associated with the formation of the spin-compensated state. Figure 6 illustrates that (above T_c) it is quite possible to mistake the impurity-spin heat capacity contributions for an enhanced γ-value.

The Ce concentration independence of the 2 kOe $\Delta C/c$ data of the 0.64 and 0.193 at.% Ce alloys compared to the corresponding data for the 0.906 at.% Ce alloy (via the curves labelled c in Fig. 4 and Fig. 5) provided the evidence that these alloys are characterized by single-impurity behavior. However, the $\Delta C/c$ data of the alloys in 2 kOe do exhibit slight systematic shape differences whose possible origin will now be speculated upon. Although the temperature of the 2 kOe excess heat capacity peak, T_p(2 kOe), remains constant for the three alloys, the height and sharpness of the peaks increase as the Ce concentration decreases. Bloomfield and Hamann found that for a given T_K-value, large increases in the Fermi temperature, T_F, produced slight increases in their calculation of $\Delta C/c$ in the vicinity of T_p. (For example, a factor of five increase in T_F increased their $\Delta C/c$ peak height approximately 3%.) Assuming the validity of this aspect of their calculation (which is not physically obvious), the magnitude

of the variation in T_F with alloying necessary to explain the experimental shape differences in 2 kOe precludes this from being a reasonable explanation. It does appear possible however, that internal strains, produced by alloying, can create a distribution of characteristic ordering temperatures--due to the pressure sensitivity of the magnetic properties of Ce--which tend to smear the impurity spin-ordering anomaly as the Ce concentration is increased. This hypothesis has not been quantitatively tested. Another possible explanation is that slight impurity-impurity interaction contributions to $\Delta C/c$ might superimpose on the dominant single-impurity behavior of the alloys. While this possibility cannot be ruled out, the low value of the magnetic-ordering temperature, T_M, for pure $CeAl_2$ of approximately 3.4 K suggests that for the Ce concentrations of the alloys under consideration, the relevant T_M-values are probably below the lowest temperatures experimentally accessible.[74] However, inhomogeneities presumably could create local regions within an alloy where impurity-impurity interactions might compete with the single impurity spin-ordering process.

2. On the Definition of T_K

Before estimates of T_K can be made and compared with each other, it must be appreciated that T_K is not a sharply defined temperature. The physical properties of systems exhibiting a Kondo effect tend to vary smoothly and gradually from above T_K to 0 K. The Kondo temperature, rather, provides an indication of the temperature scale at which the coupling between the impurity spin and the conduction-

electron spin density in the vicinity of the impurity becomes significant. This in turn depends on the physical property under consideration, and on the assumptions of the theoretical model used in its evaluation. (In this spirit, the conventional definition of T_K appearing in Eq. (1) uses, rather than an equality sign, a symbol denoting that T_K "is of the order of" .... Even with this qualification, Eq. (1) is not without its serious critics,[75])

In the (La,Ce)Al_2 alloys studied, the temperature of the peak in the excess heat capacity anomaly associated with the Kondo effect in zero field, $T_p(0)$, is 0.14 K. Bloomfield and Hamann[10] indicate that $T_p(0)$ occurs at $T_K/3$; hence T_K is 0.42 K. The calorimetrically determined T_K should be the same as that obtained from resistivity measurements analyzed within the context of Hamann's theory.[76] This has been experimentally verified in the system CuCr.[77,78] Recent resistivity measurements on a 0.63 at.% Ce (La,Ce)Al_2 alloy, however, have been interpreted as being consistent with a T_K of approximately 1.0 K when compared with Hamann's resistivity expression.[79] However, taking proper account of the host and impurity potential-scattering contributions to the resistivity, and then fitting the data above T_K to Hamann's expression might reduce the discrepancy with the calorimetrically determined T_K-value, assuming that impurity-impurity interaction effects are not important in this sample.

Riblet and Winzer, and Maple et al. have estimated T_K for the system (La,Ce)Al_2 based on an expression for the initial depression of T_c obtained using the temperature-dependent pair-breaking parameter

of the MHZ theory.[31,32,21] This T_K is 0.089 K, using an electronic density of states value of 2.05 states of one spin direction per eV per La atom, obtained from the γ_n-value of this study and by Luengo et al. and using the initial dT_c/dc obtained by Maple et al.[32,33] In another estimate of T_K, Maple et al. empirically deduced the temperature dependence of the pair-breaking parameter, α, above 0.13 K. Although below 0.26 K pair-breaking interactions were tending to saturate in strength, by 0.13 K α still did not exhibit a maximum. Since in the MHZ theory pair-breaking interactions are strongest at T_K, they concluded that T_K is less than 0.1 K.[32] This estimate is perfectly consistent with the 0.089 K estimate of T_K also made within the context of the MHZ theory.

3. High Field Behavior and the g-factor

In the presence of an externally applied magnetic field, impurity spin ordering in a dilute magnetic alloy will be modified. As the external field strength increases the impurity spins will tend to couple non-cooperatively to the external field, hence zero-field spin-ordering processes will tend to be suppressed. In a large field (i.e. $g\mu_B H > k_B T_K$ or $k_B T_M$, where H is the strength of the externally applied field, μ_B is the Bohr magneton, and g is the spectroscopic splitting-factor) $g\mu_B H$ will tend to define the energy-level splitting of the impurity spin system. Since the temperature of the heat capacity peak for a non-cooperative spin-ordering anomaly is proportional to the energy-level splitting, it will tend also to be proportional to H, assuming the external field does not significantly admix the levels

of interest with higher-lying levels. Hence in large magnetic fields it should be possible to estimate the g-factor from the temperature of the peak in the spin-ordering heat capacity anomaly.

For the (La,Ce)Al_2 alloys under consideration, the 20 kOe and 38 kOe data appear to be suitable for this type of analysis: From Figs. 3-5 it is clear that the 20 and 38 kOe fields have quite dramatically perturbed the formation of the spin compensated state. Using the T_K-value of 0.42 K and temporarily assuming a free-spin g-factor of 2, $g\mu_B H/k_B T_K$ is approximately 6 and 12 in 20 kOe and 38 kOe, respectively. It is further corroborated that these fields are strong enough essentially to determine the level splittings of the impurity spin system, by the observation that from the experimental value of the temperature of the 20 kOe $\Delta C/c$ peak of 0.63 K, the 38 kOe $\Delta C/c$ peak temperature of 1.2 K is correctly predicted: $T_p(38\ \text{kOe}) = (38/20)(0.63) = 1.2$ K. For a spin 1/2 Schottky system[80] the level splitting $g\mu_B H$ is equal to 2.40 $k_B T_p$; hence g is equal to 1.1. Using high-field CuCr (T_K = 2.1 K) excess heat capacity data and the appropriate level-splitting relation for a spin 3/2 Schottky system, a g-factor of 2.0 is obtained.[78] This lends support to the approach taken here for obtaining g-values, since the g-factor for Cr in dilute CuCr is known[81] to be 2.0. In both CuCr and (La,Ce)Al_2 the 38 kOe excess heat capacity anomalies are broader than, and their peak heights are lower than that for the appropriate Schottky anomalies (for which the peak heights would be 6.18 and 3.64 J/K mole, respectively),

hence memory of cooperation persists in these fields.

The g-factor for (La,Ce)Al_2 of 1.1 is approximately 80% of the $|g| = (5/3)\ g_J = 10/7$ theoretically obtained for the ground-state doublet of cubic Ce metal, where g_J is the Landé g-factor for the $4f'(^2F_{5/2})\ Ce^{+3}$ ground term.[28] The differences are presumably due to the dissimilar immediate environments.[82] Using the g-factor for (La,Ce)Al_2, the effective moment, μ_{eff}, in the limit $T \to 0$ K ($g\sqrt{S(S+1)}\ \mu_B$) of 0.95 μ_B is consistent with the value 0.87 μ_B (accurate to approximately 2%) obtained from extrapolations from above 1 K of the magnetic susceptibility of samples of comparable Ce concentrations to those studied here.[26,27] Hence the apparent loss of approximately 30% of μ_{eff} as $T \to 0$ deduced from the susceptibility measurements above 1 K and conjectured as being evidence of a Kondo effect seems largely attributable to the use of an incorrect g-factor.

C. Superconducting-State Alloy Behavior

1. The 0.193 at.% Ce Alloy

In Section IV-D it was demonstrated that for the 0.193 at.% Ce alloy in zero field, impurity spin ordering occurs at lower temperatures in the superconducting state than in the normal state. The total entropy difference between the superconducting state and the normal state, evaluated between T_ℓ, the lowest temperature for which there is experimental data, and T_c, is dominated by the impurity spin contributions and provides a measure of the temperature-depression of impurity spin ordering. The total entropy difference, $(S_n - S_s)\Big|_{T_\ell}^{T_c}$ divided by Ce concentration is positive and approximately 38% of $R\ell n2$. In the normal state in this temperature interval approximately 57% of the $R\ell n2$ entropy of the impurity spin system is removed (based on graphical integration of curve d of Figs. 3-5). If the difference between $S_{En}(T_\ell)$ and $S_{Es}(T_\ell)$ is neglected, this indicates that in the temperature interval between T_ℓ and T_c only approximately one-third of the impurity-spin entropy is removed when the host is superconducting compared to when it is normal. Assuming the shape of the heat capacity anomaly associated with the formation of the spin-compensated state is preserved in the superconducting host, this suppression of spin ordering corresponds to a reduction in T_K by a factor of approximately 6. Taking into account that

$$(S_{En} - S_{Es})\Big|_{T_\ell}^{T_c} = [S_{Es}(T_\ell) - S_{En}(T_\ell)] < 0$$

would tend to reduce the estimate of T_K in the superconducting state.

Attempts were made to separate the conduction-electron contribution from the impurity-spin contribution to the zero-field heat capacity of the 0.193 at.% Ce alloy. Referring to Fig. 6, it is reasonable to assume that C_{Es} dominates $C-C_L$ near T_c, and that at lower temperatures the impurity spin contribution becomes increasingly important. Assuming that C_{Es}/T is zero at 0 K and increases smoothly with temperature with positive curvature, at least below 1 K, and asymptotically approaches $(C-C_L)/T$ as T_c is approached, it was found, by graphical integration, that $S_{Es}(T_c) < S_{En}(T_c)$. This suggests that the above representation of C_{Es} is unrealistic and that there are significant contributions to C_{Es} at low temperatures which have not been taken into consideration. For example, C_{Es} could be linear in the low temperature limit, with $C_{Es}/T \to \gamma_s$ as $T \to 0$, as might be expected for a gapless superconductor. From the γ_s-value of 1.9 mJ/K^2 mole estimated by Luengo et al. for this alloy using an unusual graphical decomposition of $(C-C_L)/T$ (see Ref. 33 for details), a reasonable representation of C_{Es}/T can be constructed, by a similar procedure to that outlined above for the $\gamma_s = 0$ case, for which the entropy constraint $S_{Es}(T_c) = S_{En}(T_c)$ is satisfied. Hence, within this framework, a γ_s of 1.9 mJ/K^2 mole appears to be plausible.

Further attempts were made to separate C_{Es} from the impurity spin heat capacity by least-squares fitting the low-temperature data assuming 1) $C_{Es} \to \gamma_s T$ as $T \to 0$, and 2) the impurity-spin heat capacity contribution retains its normal-state temperature dependence

of approximately $T^{-0.6}$. For a representative fit below 1 K to the equation:

$$C-C_L = \beta T^{-0.6} + \gamma_s T + \beta_s T^3 \quad , \tag{12}$$

where the $\beta_s T^3$ term was retained to help represent C_{Es} at the higher temperatures, the approximate values of the coefficients are $\beta = 0.37$, $\gamma_s = 1.2$, and $\beta_s = 3.7$ in mJ units. The r.m.s. deviation from the fit was less than 2%, however, the fractional deviations to the fit showed some systematic behavior. In other fits with varied temperature ranges, and for which an additional term was included to help represent C_{Es} at the higher temperatures, the β- and γ_s-coefficients remained essentially constant. Plotting the $\beta T^{-0.6}$ impurity-spin heat capacity contribution as $\Delta C/c$ vs T and shifting the temperature scale to fit curve d of Figs. 3-5, a reduction in T_K of approximately a factor of 8 was found, relative to its normal-state value. However, for the decomposition of $C-C_L$ represented by Eq. (12), the quantity $S_{Es}(T_c)$ is still less than $S_{En}(T_c)$. It is plausible that the entropy constraint at T_c is not satisfied because γ_s was underestimated.

In the next attempt to separate C_{Es} from the impurity-spin heat capacity, a γ_s-value was specifically chosen to help ensure that the conduction-electronic entropy constraint at T_c is satified. In order to facilitate this, the impurity-spin heat capacity contribution was allowed to deviate from its normal-state temperature dependence. In this case:

$$C-C_L = \beta T^{-m} + \gamma_s T + \beta_n T^n \quad , \tag{13}$$

and the first term on the right is assumed to be the impurity spin contribution. The parameters β and m were graphically evaluated from the intercept and slope, respectively, of a straight line through a low-temperature log $(C-C_L-\gamma_s T)$ vs log T plot, and the parameters β_n and n were evaluated similarly from a log $(C-C_L-\gamma_s T-\beta T^{-m})$ vs log T plot. A representative analysis gave, for a choice of γ_s = 2.3 mJ/K^2 mole, the following approximate parametric values: β = 0.21, m = 0.84, β_n = 2.8, and n = 4.2. For this particular case $S_{Es}(T_c)$ was within 1.5% of $S_{En}(T_c)$. For choices of γ_s as large as 2.3 mJ/K^2 mole, however, the log-log plots exhibited significant curvature and the parameter m was very sensitive to small variations in γ_s(i.e. increasing γ_s to 2.4, increased m to 0.97). Hence, this decomposition provides somewhat ambiguous quantitative information. Clearly, however, within this framework, m is much less than 2.

For this alloy, the appearance of significant contributions to C_{Es} at low temperatures cannot be explained by the BCS and AG theories. The AG theory predicts $\gamma_s > 0$ at very high impurity concentrations, however for low concentrations γ_s will be zero and conduction-electron states will not be present at low temperature near the Fermi energy. Of those attempts, presented above, to separate C_{Es} from the impurity spin heat capacity contribution which were plausible, a $\gamma_s > 0$ was assumed to exist. However, due to the lack of theoretical expressions necessary to help guide the analyses of the heat capacity into meaningful component contributions, none of the above decompositions can be claimed to have characterized the temperature-dependences of the

of the superconducting-state heat capacity of either the conduction-electron system or the impurity-spin system. For instance, if as in the theory of MHZ for $J < 0$ and $T_K \sim T_{C_o}$, impurity bands grow from within the energy gap of the pure superconductor, then it appears that C_{Es}/T may be increasing or decreasing at low temperature and C_{Es} may not be characterized by a linear temperature dependence. Similarly, it was necessary to invoke an unusual low-temperature heat capacity behavior for the $LaAl_2$ which actually contains 0.01-0.02 at.% Ce, in order to satisfy the conduction-electronic entropy constraint at T_c.

The reduction of T_K in a superconducting host relative to a normal host (for $T_K < T_{Co}$) at low impurity concentrations may indicate that conduction-electron states are not as readily available for spin-compensation in the superconductor. Physically this seems reasonable since at low impurity concentrations the conduction-electron states are primarily participating in the Cooper pairing. The γ_s-value might be expected to provide an indication of the availability of conduction-electron states for spin compensation. However, if a γ_s-value of 2.3 or 1.9 mJ/K^2 mole is taken as a measure of $N(E_F)$ in the superconducting state, and if an equality of the form of Eq. (1) is assumed, for the approximately one order of magnitude that T_K is reduced in the transition to the superconducting state, $N(E_F)|J|$ is reduced by a factor of only 1.2, although $N(E_F)$ is reduced by a factor of 4 or 5. (This comparison is based on an assumed T_F of the order of 5×10^4 K, but it is not sensitive to the value of T_F). Using this

approach a γ_s-value of approximately 8 mJ/K^2 mole would be necessary to account for the estimated reduction in T_K.

LaCe is another superconductor whose properties are thought to be influenced by a Kondo effect. Detailed comparisons between the (La,Ce)Al_2 and LaCe systems are precluded, however, since experiments on the latter are usually performed on mixed phase samples, due to the similarity in stability of the cubic and hexagonal phases of La. However in the LaCe system, at very low Ce concentrations the existence of low energy excitations at low temperatures have been inferred from both heat capacity and tunneling experiments. Hence, in the dilute limit there is general agreement in the superconducting behavior of these closely related systems.

2. The 0.64 at.% Ce Alloy

The critical concentration of Ce that destroys superconductivity at all accessible temperatures in homogeneous (La,Ce)Al_2 alloys is approximately 0.7 at.% Ce. Superconductivity has been detected in this alloy system above this critical-concentration-value, however mutual-inductance measurements indicate that for such cases the superconducting transitions are not fully diamagnetic. The superconductivity of such alloys is attributable to concentration inhomogeneities which locally reduce the Ce concentration below the critical value. Once such a sample has been property annealed superconductivity disappears.

The 0.64 at.% Ce alloy closely approaches the critical-concentration-value. The superconducting properties of this alloy would be expected to be characterized by gapless behavior at all temperatures according to the AG theory, for which γ_s would be $\gtrsim 0$. A comparison of the 0 and 0.5 kOe heat capacity data (see Fig. 4) indicates that the superconducting-state heat capacity is quite similar to that of the normal state. Thus the superconducting-state can be qualitatively characterized as being representative of an extreme gapless limit, for which γ_s would be $\lesssim \gamma_n$. Figure 4 also indicates that there is no feature in the zero-field heat capacity in the vicinity of T_{C_2}, the temperature that characterizes the inductively-detected, broad transition back into the normal state upon cooling. However, the 0 and 0.5 kOe $\Delta C/c$ data merge as T_{C_2} is approached from higher temperatures. (At the lowest temperatures a small field enhancement effect is observed in 0.5 kOe as in Fig. 3 for the 0.906 at.% Ce alloy.) Perhaps the sample re-enters the normal state on cooling in the vicinity of T_{C_2} with C_{Es}/T increasing to the value γ_n. Then all three of the samples that exhibit superconductivity may have the anomalous property that C_{Es}/T increases at low temperature. In the MHZ theory this would be due to the existence of quasibound states deep in the energy gap of the pure superconductor.

For the 0.193 at.% Ce alloy spin-ordering was depressed in temperature for the superconducting host relative to the normal host. For the 0.64 at. % Ce alloy any reduction in T_K at the transition to the superconducting state would probably lie within the experimental error limits to which it could be estimated.

REFERENCES

1. C. Kittel, in Solid State Physics, edited by F. Seitz, D. Turnbull, and H. Ehrenreich (Academic Press, New York, 1968) Vol. 22.
2. W. Marshall, Phys. Rev. 118, 1519 (1960).
3. See for instance, N. E. Phillips, Critical Reviews in Solid State Physics, 467, (1971).
4. J. Kondo, Progr. Theoret. Phys. (Kyoto) 34, 505 (1964).
5. See for instance, A. A. Abrikosov, Introduction to the Theory of Normal Metals (Academic Press, New York, 1972) p. 57.
6. Y. Nagaoka, Phys. Rev. 138, A1112 (1965).
7. J. C. F. Brock, J. C. Ho, G. P. Schwartz, and N. E. Phillips, Solid State Commun. 8, 1139, (1970).
8. Y. Nagaoka, Progr. Theoret. Phys. (Kyoto) 37, 13 (1967).
9. B. B. Triplett and N. E. Phillips, Phys. Rev. Lett. 27, 1001 (1971).
10. P. E. Bloomfield and D. R. Hamann, Phys. Rev. 164, 856 (1967).
11. See for instance, A. J. Heeger, in Solid State Physics, edited by F. Seitz, D. Turnbull, and H. Ehrenreich (Academic Press, New York, 1969) Vol. 23, p. 283.
12. See for instance, M. B. Maple, in Magnetism: A Treatise on Modern Theory and Materials, edited by H. Suhl, (Academic Press, New York, 1973) Chapter 10.
13. B. T. Matthias, H. Suhl, and E. Corenzwit, Phys. Rev. Lett. 1, 92 (1958).
14. J. Bardeen, N. Cooper, and J. R. Schreiffer, Phys. Rev. 108, 1175 (1957).

15. A. A. Abrikosov and L. P. Gorkov, Soviet Physics -- JETP, 12, 1243 (1961), (English translation).

16. S. Skalski, O. Betbeder-Matibet, and P. R. Weiss, Phys. Rev. 136, A1500 (1964).

17. A. Griffin, in Superconductivity, edited by P. R. Wallace (Gordon and Breach, New York, 1969) p. 577.

18. E. Müller-Hartmann, in Magnetism: A Treatise on Modern Theory Materials, edited by H. Suhl (Academic Press, New York, 1973).

19. J. Zittartz and E. Müller-Hartmann, Z. Physik 232, 11 (1970).

20. E. Müller-Hartmann and J. Zittartz, Z. Physik 234, 58 (1970).

21. J. Zittartz, Z. Physik 237, 419 (1970) and J. Zittartz, Proceedings of the Twelfth International Conference on Low Temperature Physics edited by E. Kanda (Kyoto, Japan, 1970) p. 647.

22. E. Müller-Hartmann and J. Zittartz, Phys. Rev. Lett. 26, 428 (1971).

23. E. Müller-Hartmann and J. Zittartz, Z. Physik 256, 366 (1972).

24. J. Zittartz, A. Bringer and E. Müller-Hartmann, Solid State Commun, 10, 513 (1972).

25. E. Müller-Hartmann and J. Zittartz 11, 401 (1972).

26. M. B. Maple and Z. Fisk, Proceedings of the Eleventh International Conference on Low Temperature Physics, edited by J. F. Allen, D. M. Findlayson and D. M. McCall (St. Andrews, Scotland, 1968) Vol. 2, p. 1288.

27. M. B. Maple, Ph.D. thesis (University of California, San Diego, 1969).

28. T. Murao and T. Matsubara, Progr. Theoret. Phys. (Kyoto) 18, 215 (1957).

29. M. B. Maple, Solid State Commun. 8, 1915 (1970).

30. M. B. Maple and T. F. Smith, Solid State Commun. 7, 515 (1969).

31. G. Riblet and K. Winzer, Solid State Commun. 9, 1663 (1971).

32. M. B. Maple, W. A. Fertig, A. C. Mota, L. E. DeLong, D. Wohlleben, and R. Fitzgerald, Solid State Commun. 11, 829 (1972).

33. C. A. Luengo, M. B. Maple and W. A. Fertig, 11, 1445 (1972).

34. C. A. Luengo, Ph.D. thesis (Universidad Nacional de Cuyo, Bariloche, Argentina, 1972).

35. Cryocal, Inc., Riviera Beach, Florida.

36. R. A. Erickson, L. D. Roberts and J. W. T. Dabbs, Rev. Sci. Instr. 25, 1178 (1954).

37. Two-Phase Lock-In Amplifier (Model JB-6), Princeton Applied Research, Princeton, New Jersey.

38. Alleghany Ludlum Steel Corporation, Pittsburgh, Pennsylvania 15222.

39. Engelhard Industries Incorporated, Research and Development Division, 497 Delancy Street, Newark, New Jersey 07105.

40. J. C. Ho and N. E. Phillips, Rev. Sci. Instr. 36, 1382 (1965).

41. D. C. Ginnings and E. D. West, Rev. Sci. Instr. 35, 965 (1964).

42. Model CFC-100, Magnion, Incorporated, 144 Middlesex Turnpike at Third Avenue, Burlington, Massachusetts 01804.

43. B. B. Triplett, Ph.D. thesis (University of California, Berkeley, 1970). [UCRL-19672 (unpublished)].

44. General Electric Company, Insulating Materials Department, Schenectady, New York 12305.

45. Emerson and Cuming, Inc. Dielectric Materials Division, Canton, Massachusetts

46. G. L. Salinger and J. C. Wheatley, Rev. Sci. Instrum. 32, 872 (1961).

47. D. L. Martin, Phys. Rev. 141, 576 (1966).

48. Cominco Amercan, Inc., Building 101, Spokane Industrial Park, Spokane, Washington 99216.

49. J. L. Cude and L. Finegold, Cryogenics 11, 394 (1971).

50. J. T. Hessels, Cryogenics 11, 483 (1971).

51. N. E. Phillips, Phys. Rev. 114, 676 (1959).

52. Apiezon Products Limited, 8 York Road, London, England (sold by James G. Biddle Company, Township Line and Jolly Roads, Plymouth Meeting, Pennsylvania).

53. Shell Chemical Company, Houston, Texas (repackaged by E. V. Roberts and Associates, Inc., 9601 W. Jefferson Blvd., Culver City, California 90230).

54. The solenoid was designed by the late A. Buhl.

55. NEMA G-10 tubing, purchased from Synthane Taylor, 1373 Laurel Street, San Carlos, California 94070.

56. Norton Company, Supercon Division, 9 Erie Drive, Natick, Maine 01760.

57. Airco Kryoconductor Superconducting Wire, Air Reduction Company, Incorporated, Mountain Avenue, Murray Hill, New Jersey 07971.

58. Pressure-welding was suggested by C. R. Grahmann (private communication).

59. D. L. Martin, Phys. Rev. 170, 650 (1968).

60. R. A. Fisher, G. E. Brodale, E. W. Hornung and W. F. Giauque, Rev. Sci. Instr. 39, 108 (1968).

61. E. W. Hornung, R. A. Fisher, G. E. Brodale, and W. F. Giauque, J. Chem. Phys. 50, 4878 (1969).

62. R. C. Zeller and R. O. Pohl, Phys. Rev. B 4, 2029 (1971).

63. W. F. Giauque, R. A. Fisher, E. W. Hornung and G. E. Brodale, J. Chem. Phys. 58, 2621 (1973).

64. P. W. Anderson, B. I. Halperin, and C. M. Varma, Phil. Mag. 25, 1 (1972).

65. C. Kittel and A. A. Maradudin, (unpublished).

66. The BCS heat capacity jump was incorrectly reported in Ref. 14.

67. For a tabular representation of a BCS superconducting-state heat capacity see: B. Mühlschlegel, Z. Physik 155, 313 (1959).

68. R. E. Hungsberg and K. Gschneidner, Jr., J. Phys. Chem. Solids 33, 401 (1972).

69. J. M. Machado da Silva, J. M. McDermott and R. W. Hill, J. Phys. C: Solid State Phys. 5, 1573 (1972).

70. P. W. Anderson, J. Phys. Chem. Solids 11, 26 (1959).

71. D. Markowitz and L. P. Kadanoff, Phys. Rev. 131, 563 (1963).

72. J. R. Clemm, Ph.D. thesis (University of Illinois, Urbana, 1965).

73. See Ref. 18.

74. See for instance, R. W. Hill and J. M. Machado da Silva, Phys. Lett. 30A, 13 (1969).

75. P. W. Anderson, Comm. Sol. State Phys. 5, 73 (1973).

76. D. R. Hamann, Phys. Rev. 158, 570 (1967).

77. For a discussion of the analysis of the resistivity measurements on CuCr see Ref. 11.

78. B. B. Triplett and N. E. Phillips, Proceedings of the Twelfth International Conference on Low Temperature Physics, edited by E. Kanda (Kyoto, Japan, 1970) p. 747.

79. W. Felsch and K. Winzer, Solid State Commun. 13, 569 (1973).

80. See for instance, A. M. Rosenberg, Low Temperature Solid State Physics, Oxford, Clarendon Press (1963) pp. 23-30.

81. See, for instance, Ref. 11, p. 336.

82. J. A. White, H. J. Williams, J. H. Wernick and R. C. Sherwood, Phys. Rev. 131, 1039 (1963).

FIGURE CAPTIONS

Fig. 1. The zero-field heat capacity. From top to bottom the smooth curves represent the data for the 0.0, 0.906, 0.193 and 0.64 at.% Ce samples.

Fig. 2. The electronic heat capacity of $LaAl_2$. The horizontal line represents $\gamma_n = 9.65$ mJ/K^2 mole. The curve represents a BCS superconducting-state electronic heat capacity for $T_c = 3.307$ K and $\gamma_n = 9.65$.

Fig. 3. The excess heat capacity of the 0.906 at.% Ce (La,Ce)Al_2 sample per mole of Ce. Curves a, b and c represent the 38,20 and 2 kOe data. Curve d, shifted in temperature and scaled to give an entropy of R ℓn 4 fits the spin-compensated state heat capacity anomoly of CuCr in zero field. Curve d originally derives from the calculations of Bloomfield and Hamann. The error bars represent the effect of a 1 % error in the total heat capacity measured.

Fig. 4. The excess heat capacity of the 0.64 at.% Ce (La,Ce)Al_2 sample per mole of Ce. Curves a through d are reproduced from Fig. 3. The error bars represent the effect of a 1 % error in the total heat capacity measured. The vertical arrows indicate the positions of the magnetically detected T_{c_1} and T_{c_2}.

Fig. 5. The excess heat capacity of the 0.193 at.% Ce (La,Ce)Al_2 sample per mole of Ce. Curves a through d are reproduced from Fig. 3. The error bars represent the effect of a 1 % error in the total heat capacity measured.

Fig. 6. The zero-field heat capacity of the 0.193 at.% Ce, (La,Ce)Al_2 sample with the lattice contribution subtracted. The horizontal bars on the data points near T_c = 2.83 K indicate the width of the measured data points. The horizontal line represents γ_n = 9.65 mJ/K^2 mole. The dot-dashed curve represents the smoothed, zero-field, excess heat capacity of the 0.906 at.% Ce sample scaled in concentration to 0.193 at.% Ce. The dashed curve is the sum of the dot-dashed curve plus the horizontal line and it represents a combined zero-field, normal-state conduction-electronic and impurity-spin heat capacity.

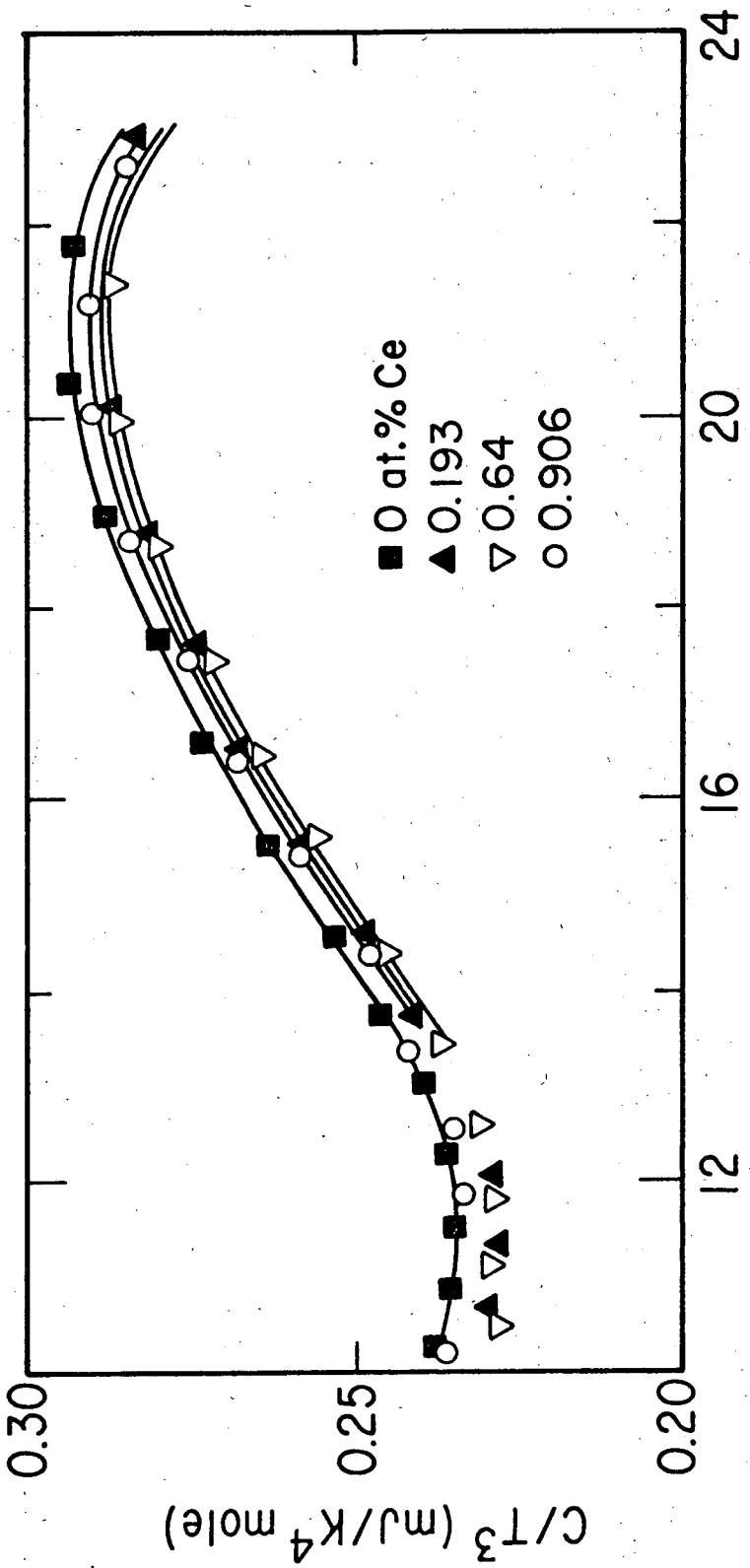

XBL 7311-6629

Fig. I-1.

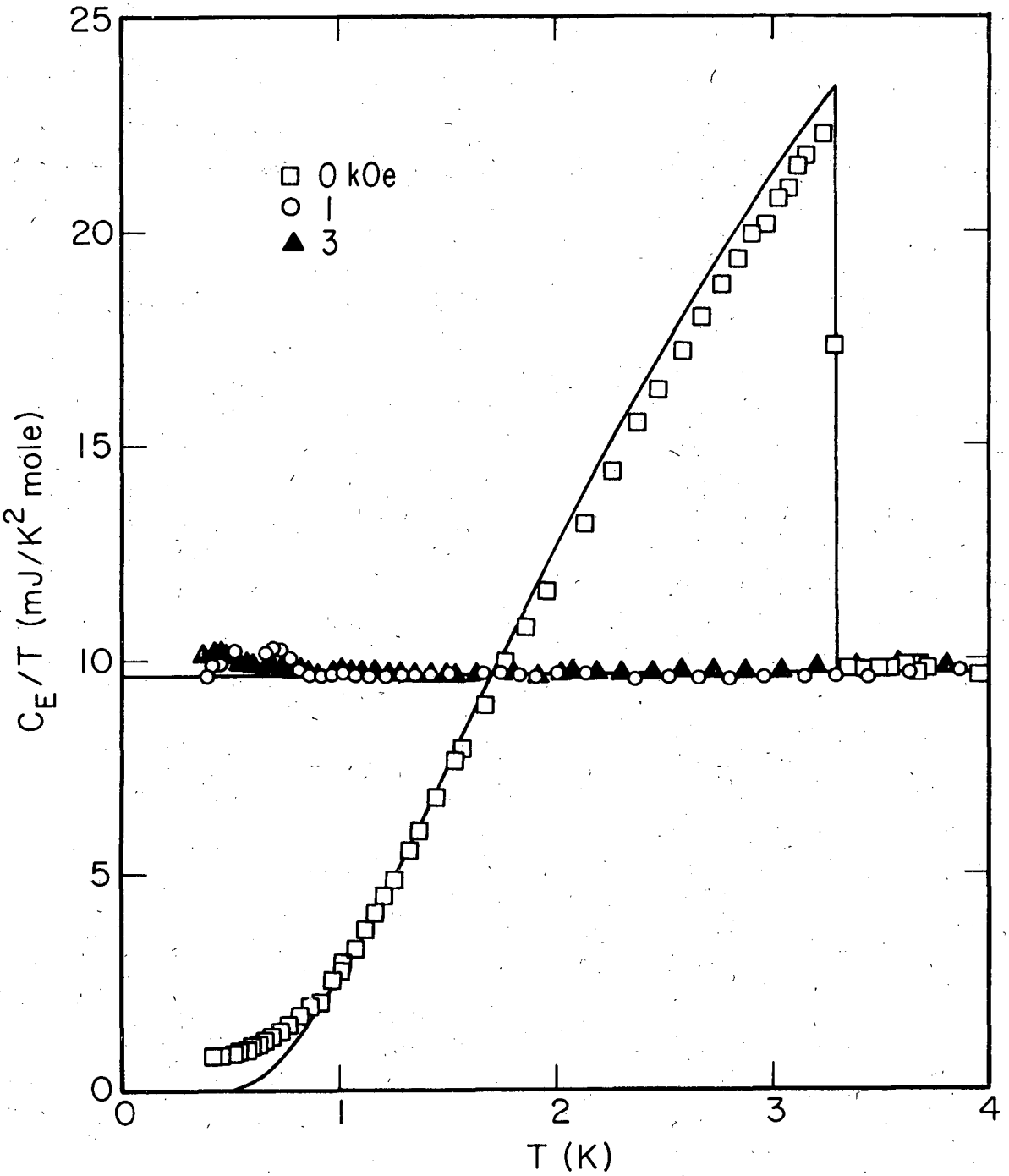

Fig. I-2.

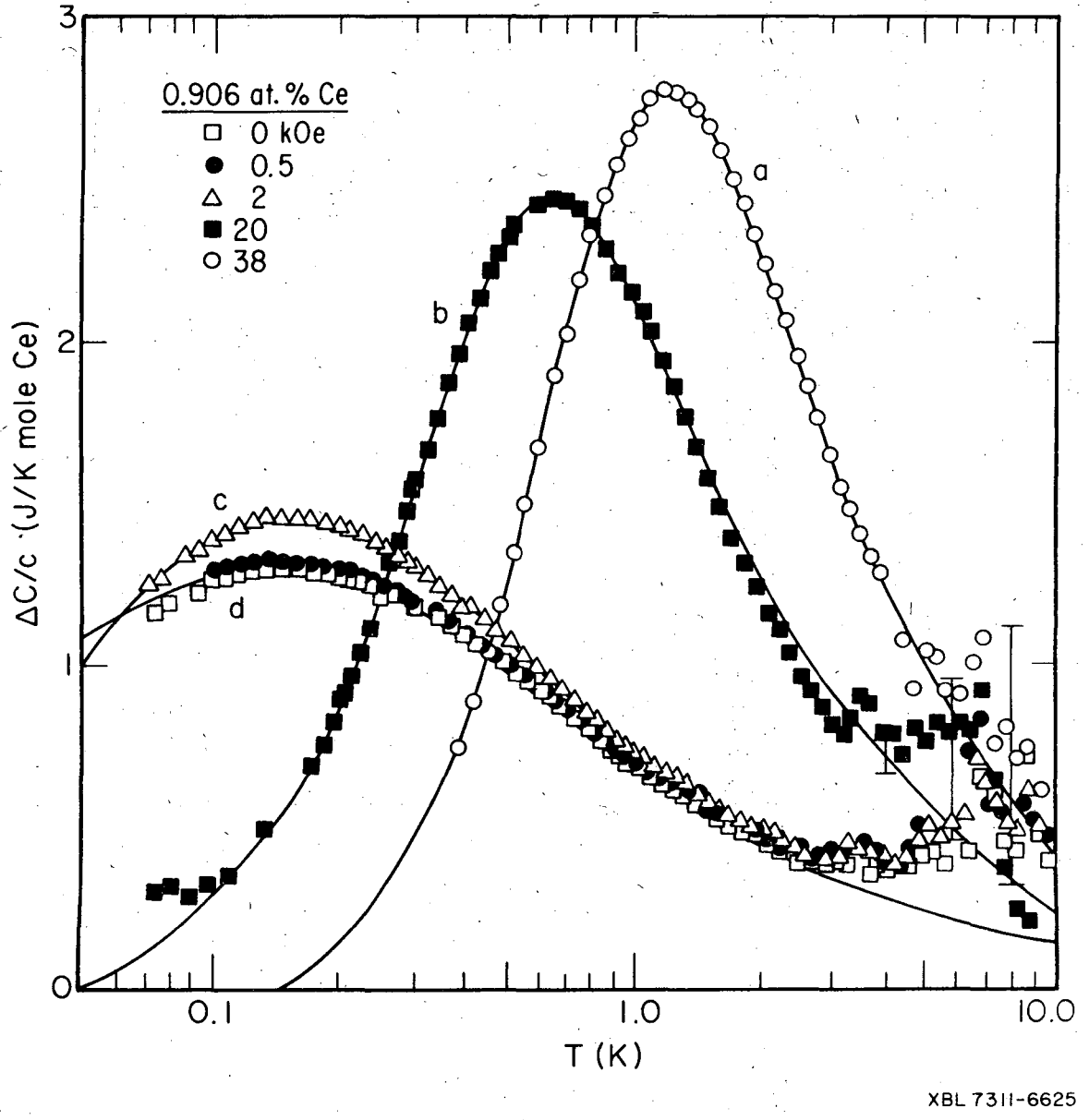
0.906 at. % Ce
0 kOe
0.5
2
20
38
a
b
c
d
ΔC/c (J/K mole Ce)
T (K)
0.1
1.0
10.0
0
1
2
3
XBL 7311-6625

Fig. I-3.

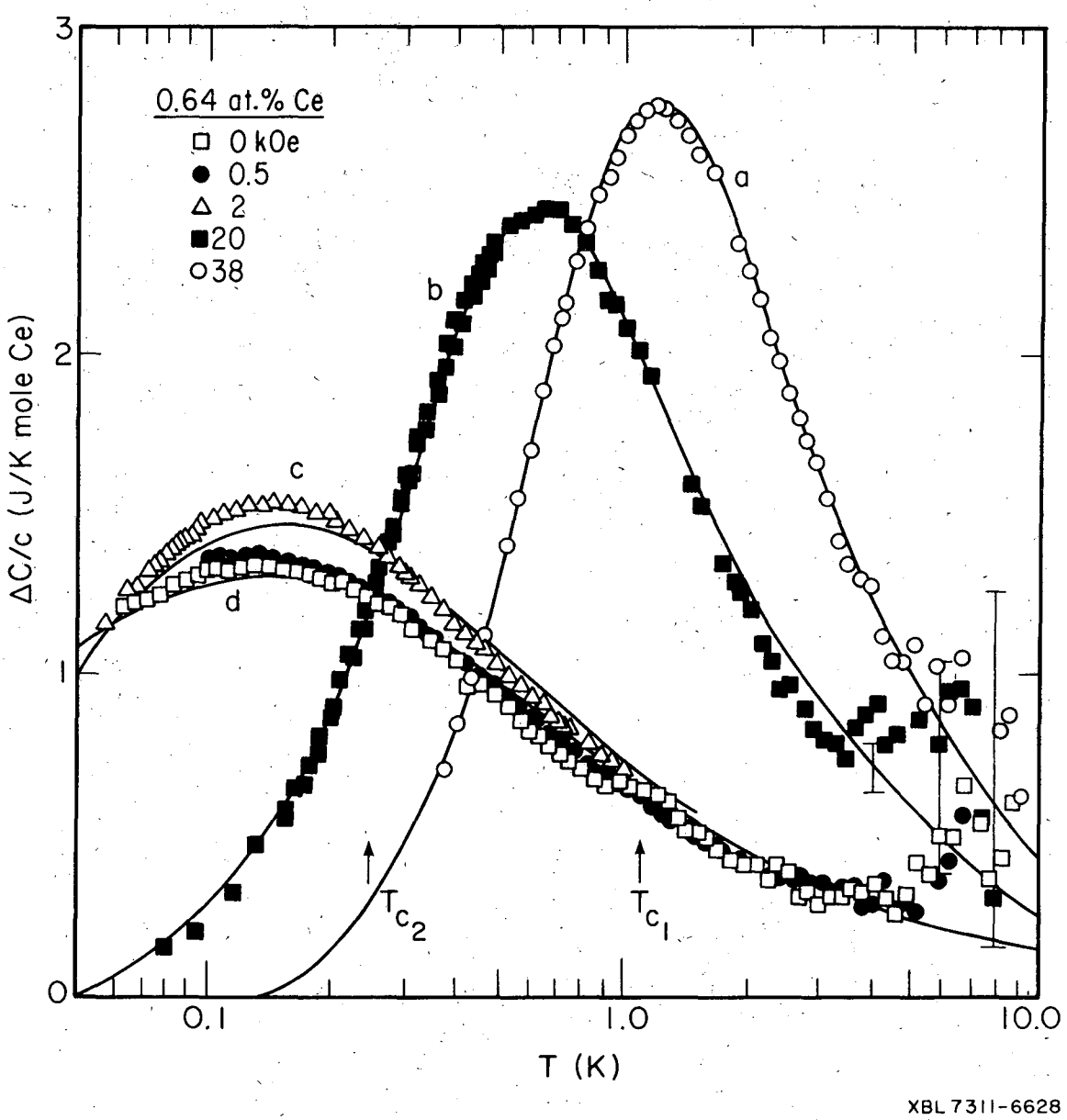
0.64 at.% Ce
0 kOe
0.5
2
20
38
a
b
c
d
T_{c_2}
T_{c_1}
ΔC/c (J/K mole Ce)
T (K)
0
1
2
3
0.1
1.0
10.0
XBL 7311-6628

Fig. I-4.

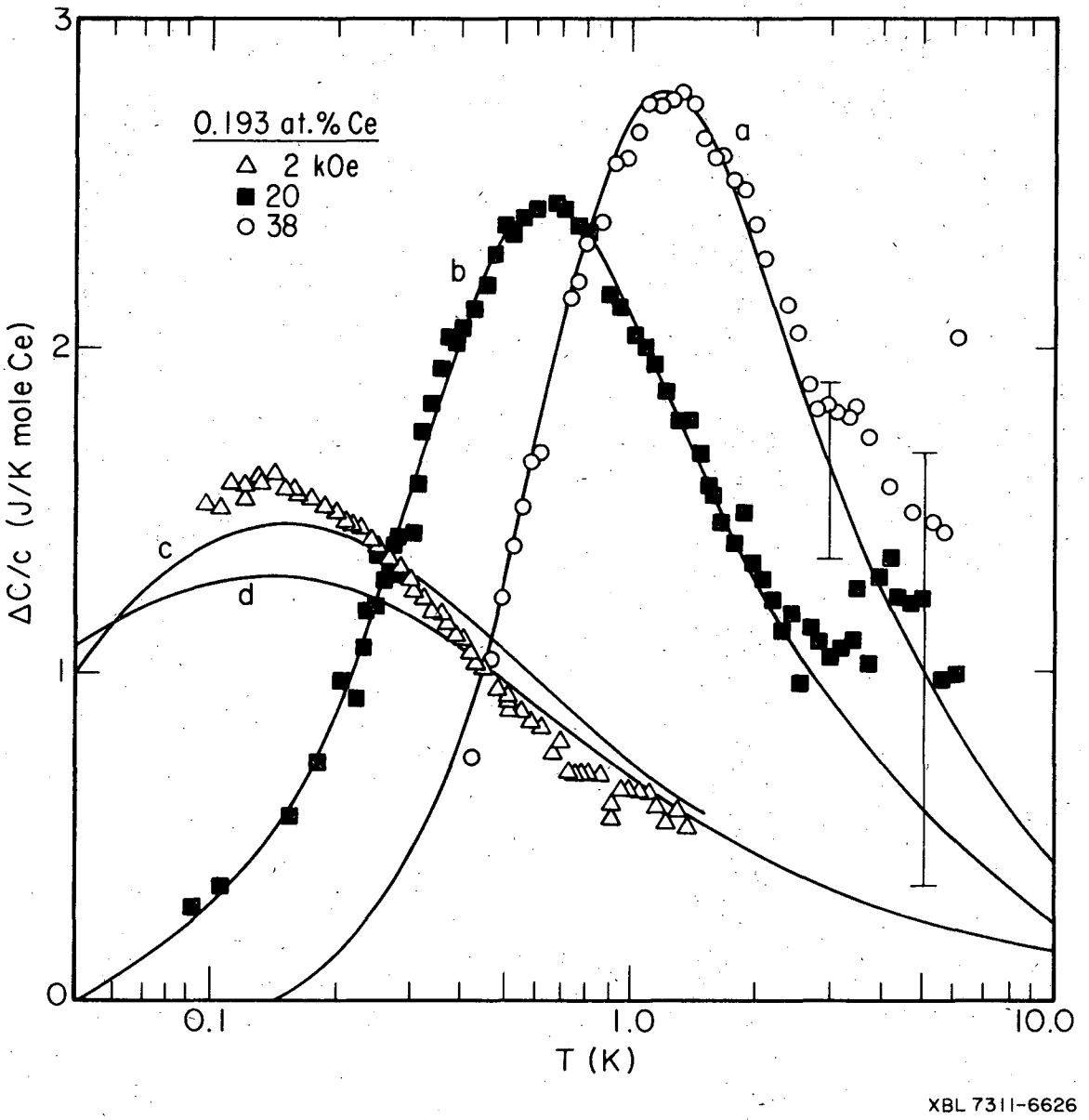
0.193 at.% Ce
△ 2 kOe
■ 20
○ 38
a
b
c
d
ΔC/c (J/K mole Ce)
T (K)
0.1
1.0
10.0
0
1
2
3
XBL 7311-6626

Fig. I-5.

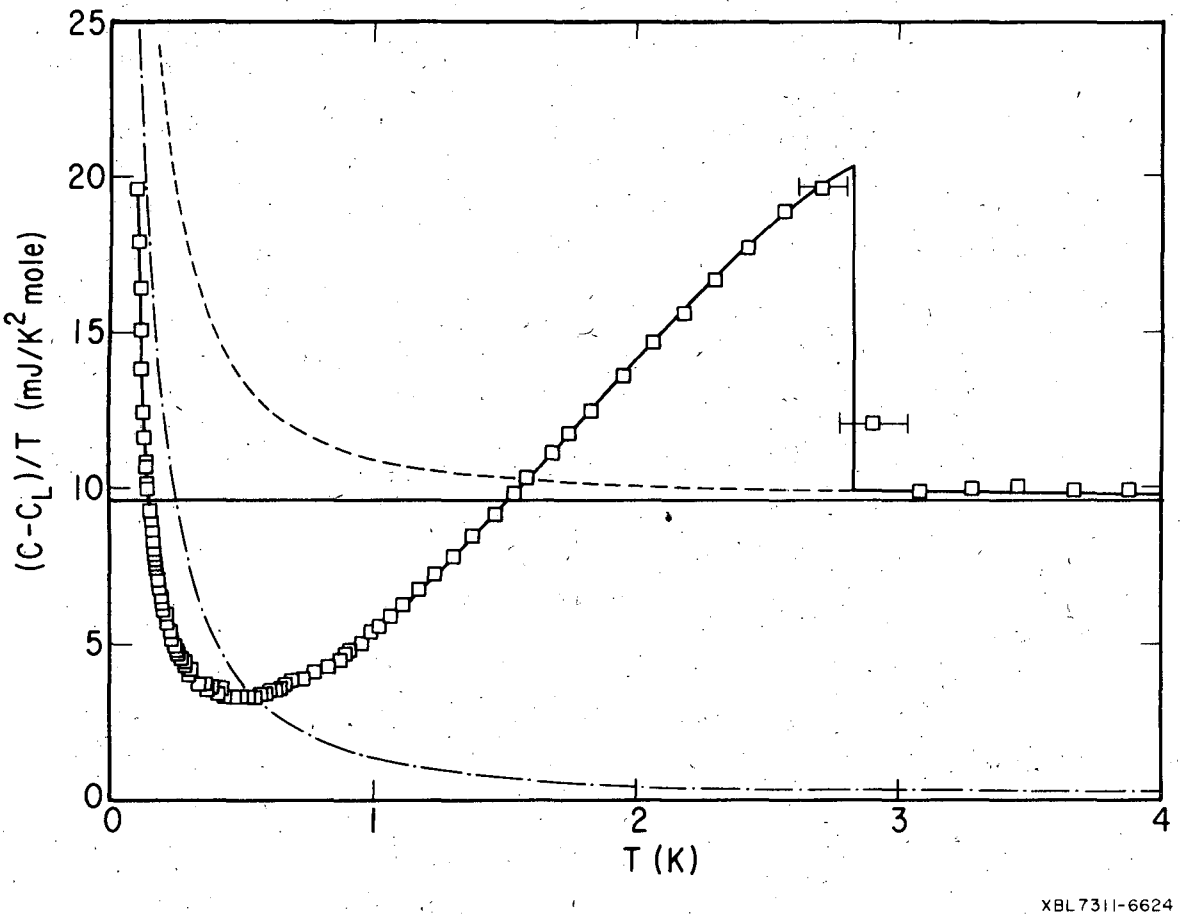

Fig. I-6.

PART TWO: α-U

I. INTRODUCTION

This study was undertaken to clarify the calorimetric properties of α-U below 1 K in order to help reveal the nature of the superconductivity of uranium metal. Magnetic measurements have consistently shown the occurrence of superconductivity in α-U at zero pressure, with T_c ranging from about 0.2 K for single crystals,[1,2] to above 1 K in some high-purity polycrystals.[3] Calorimetric studies to date, however, have failed to substantiate the existence of superconductivity in α-U at zero pressure. At 10 kbar, however, there is agreement between calorimetric and magnetic measurements. At that pressure α-U is a bulk superconductor[4] with a T_c of approximately 2 K. Hence, α-U is the most strongly pressure-enhanced superconductor known. Furthermore it has the largest deviation from the BCS isotope effect[5] with T_c proportional to approximately M^2 at 11 kbar.

When cooled slowly, α-U increases in volume[6] below 43 K. The most outstanding features accompanying this 43 K volume-minimum are sharp minima in the elastic moduli.[7,8] The most pronounced anomaly occurs in the C_{11} stiffness modulus, in the [100] crystal direction, along which the second-nearest-neighbor bond is aligned. X-ray and neutron-diffraction studies[9,10] indicate that there are no deviations from the orthorhombic structure at low temperatures, and that there is no evidence of magnetic ordering above 10 K. The orthorhombic-structure a lattice parameter increases markedly below 43 K, the b parameter increases less so, and the c parameter decreases below 43 K

at a more rapid rate than at higher temperatures. Magnetic susceptibility measurements on four high-purity single crystals indicated that there is a large anisotropic paramagnetic component present at all temperatures, that χ decreases 5% between room temperature and 4.2 K, and that below 40 K there are no increases in χ along any of the principal crystallographic axes, although there are slope changes.[11] There is a rapid drop in the Hall coefficient[12] between 40 K and 20 K. Expansion measurements indicate that rapid quenching can suppress or partially suppress the low temperature volume increase.[13,14] Depending on the cooling rate, a quenched sample can even be denser at low temperature than at 43 K. Hysteretic behavior of the electrical resistivity and of the thermopower was found to depend upon the rate of cooling below 43 K and upon whether static or dynamic measurements were being made.[15,16] The 43 K anomaly is also sensitive to alloying and to pressure. X-ray measurements[17] indicated that a 5.5 at.% Pu alloy was denser at 4.2 K than at 43 K. Np additions could also suppress the volume minimum, however for these alloys two crystallographically-distinct phases formed at low temperatures, perhaps due to impurity problems.[17] Based on the linear temperature-depression of the elastic-modulus anomalies with increasing pressure, followed up to 4 kbar, it was estimated that at approximately 12 kbar the anomalies would be suppressed.[18] At this pressure the volume minimum would also be suppressed, and the superconducting transition temperature reaches its maximum value.[19] First-order phase changes have been reported in single crystals at temperatures below 43 K. Most notably, strain-gage thermal-expansion

measurements[20] indicate abrupt discontinuities at 23 K and 37 K, however, it is not clear that these transitions are equilibrium properties of α-U. Anomalous behavior above 43 K includes an approximately 20% increase in the compressibility[21] upon cooling from approximately 80 K to 40 K. There is also a small bump in the ultrasonic attenuation[21] and a thermopower anomaly[16] at 250 K.

II. DESCRIPTION OF THE SAMPLES

Heat capacity measurements are reported for five samples. Table I contains a description of the samples including the results of the magnetically-detected superconducting transitions. Sample Ia is the purest uranium currently available. It was electron-beam zone-refined and contains less than 50 ppm impurities by weight. Its zero-pressure superconducting transition has been extensively investigated magnetically.[3] Sample Ia became Sample Ib after swaging. Polarized-light micrographs were used to characterize the grain structure of these samples. Samples IIa and IIb are two pieces cut from a large strain-annealed polycrystal designated U10 in the literature, and studied extensively at low temperatures, and as a function of pressure, both magnetically[19,22] and calorimetrically.[4,23] Sample III is a large grain-coarsened single crystal.[24] The superconducting transitions of similar single-crystals have been studied magnetically at zero pressure and up to 8 kbar.[1,2]

All three of the samples are partially depleted of ^{234}U and ^{235}U. Reducing the ^{234}U-content reduces the self-heating level since it accounts for more than half the total α-heating in natural uranium. Reducing the ^{235}U content reduces the nuclear quadrupole heat capacity.

III. EXPERIMENTAL TECHNIQUE

Heat capacities were measured between 0.1 K and 2 K in an adiabatic demagnetization cryostat by the heat pulse method using a previously calibrated Ge thermometer (Ge 644 calibrated on the laboratory scale T_δ). Thermal contact between the chrome alum cooling salt and the calorimeter was made with a Pb heat switch in parallel with a Cu shunt. The Cu shunt was designed to conduct away the alpha-decay generated heat from the sample at a temperature between 0.2 and 0.3 K. At lower temperatures the calorimeter was always on warming drifts, since the self-heating is constant and the thermal conductivity of the Cu shunt decreases with temperature. At higher temperatures the calorimeter would exhibit cooling drifts. When these cooling drifts became too steep the temperature of the cooling salt could be increased to minimize the heat flow to and from the calorimeter. The calorimeter consisted predominantly of a heavy Cu wire soldered at one end to the Pb switch and attached at the other to part of a sample. The thermometer was attached to another section of the sample with its four electrical leads fastened directly to the sample. The 4 kΩ, Pt-8%W heater was non-inductively wrapped around a copper post which was attached, along with the heater electrical leads, directly to another section of the sample. All attachments were made with GE7031 varnish and, when necessary, with small Cu wires. No attempt was made to correct for the varnish heat capacity, and hence, no significance is attributed to the observed T^3 terms in the

sample heat capacities. The empty calorimeter was calibrated in a separate run and its heat capacity assumed to be magnetic-field independent. The calorimeter was generally a small fraction of the total heat capacity measured, except in the 1.8 g single-crystal experiments, for which it was approximately 40% of the total heat capacity between 0.25 and 1 K. Since the Ge thermometer was attached directly to the sample to avoid locating it along a temperature gradient caused by α-U self-heating effects, it experienced the full magnetic field applied to the sample. It was, however, checked in an independent experiment that, for the present purposes, the thermometer retained its zero-field calibration in the low fields used in these experiments. This was accomplished by monitoring the slow warming drift of the calorimeter and cooling salt system with the Pb switch in the normal, or closed, position as magnetic fields were alternately turned on and off. Below 700 Oe there was no significant affect. Since all experiments were conducted at or below 500 Oe, the zero-field calibration could be used confidently.

Magnetic measurements to detect superconductivity were made using a 23 cps a.c. mutual-inductance bridge utilizing a variable reference mutual inductance.

IV. RESULT AND DATA ANALYSIS

Table II provides a summary of the eleven α-U heat capacity experiments. The zero-field heat capacity of all five samples appeared to exhibit superconducting transitions. Magnetic fields were applied to suppress the superconductivity, and the in-field data were least-squares fitted to the expression:

$$C = fAT^{-2} + \gamma T + B_3 T^3 \qquad (1)$$

where f is the molefraction of ^{235}U in the sample, A is the coefficient of the nuclear quadrupolar heat capacity, C_N, of pure ^{235}U, γT is the normal-state electronic heat capacity, C_{En}, and the B_3T^3 term, which is approximately 3-4% of C at 1 K for all samples, is attributed with no significance since the heat capacity of the GE7031 varnish was not corrected for. The heat capacities below approximately 0.27 K for Sample IIa in 500 Oe and for Sample III in 200 Oe are plotted in Fig. 1 as CT^2 vs T^3. The straight lines in Fig. 1 represent the first two terms on the right in Eq. (1) as $(C_N + C_{En})T^2$ vs T^3. The A-values for Samples IIa, IIb and III are tabulated in the second column of Table III. The applied fields did not fully suppress the superconductivity of Samples Ia and Ib, hence the average A-value of 10.8 mJ K/mole ^{235}U, obtained from the other three determinations, was used to represent C_N. For these two samples, C_{En} and B_3T^3 were characterized by least-squares fitting normal-state $C-C_N$ data in the 0.6-1.5 K interval for Sample Ia, and in the 0.7-2 K interval for Sample Ib. The γ-values for all five samples are tabulated in the

third column of Table III.

The electronic heat capacity of Sample Ia is plotted in Fig. 2 as C_E/T vs T, where $C_E = C - C_N - B_3T^3$. In zero field the sample clearly exhibits bulk superconductivity. The calorimetric transition begins below 0.4 K, and is broadened, presumably due to strains caused by the anisotropic thermal expansion below 43 K. Figure 3 shows the electronic heat capacity for this same sample after cold-working. There is a considerably broadened superconducting transition beginning above approximately 1 K. In 500 Oe some superconductivity persists below 0.7 K. Cold-working has increased the γ-value from 9.59 to 9.86 in mJ units. (The γ-value for Sample Ib was determined using data between 0.7 K and 2 K.) Samples IIa and IIb are smaller grained than Sample Ia, and differ from each other in that the former was heavily electro-etched and the latter was measured in a tarnished form. They both have similar onset T_c-values of approximately 0.7 K. The C_{Es} of the tarnished sample, IIb, is, however, slightly systematically enhanced in temperature compared to C_{Es} of Sample IIa, as is the γ-value and the nuclear A-values. The additional surface strain and impurities associated with the tarnishing probably account for all of these slight enhancements. Since these results indicate that C_{Es} and γ depend on the metallurgical state, which determines the degree of strain within a sample, the heat capacity of a single crystal was measured. The γ-value of the single crystal of 9.14 mJ/K^2 mole is lower than that of any of the polycrystals under consideration. The electronic heat capacity in 0 and 200 Oe appears in Fig. 5. Above

0.25 K the single crystal exhibits normal behavior. Below this temperature it appears that the zero-field data systematic increases as temperature is reduced, while the in-field data randomly scatter about the γ-value. (The large scatter at the lowest temperatures is predominantly due to the removal of the C_N-term, which becomes more than 80% of the normal-state heat capacity at 0.1 K.) It is plausible that below 0.25 K in zero-field, Sample III begins to enter the superconducting state. On a subsequent cooldown, as shown in Fig. 6, a superconducting transition was observed magnetically between approximately 0.2 and 0.45 K for this sample. The transition signal corresponded to complete flux exclusion by approximately 0.2 K, however, size and shape corrections make this uncertain by as much as 25%.

V. DISCUSSION

A) Normal-State Data

1. The Nuclear Heat Capacity

An average value of 10.8 mJ K/mole ^{235}U was obtained for the coefficient of the nuclear quadrupolar heat capacity of pure ^{235}U, based on three separate measurements of two istopically distinct samples. This value agrees with the value 10.9±0.7 mJ K/mole ^{235}U calorimetrically obtained by Dempesy et al.[25] below 0.75 K for pure ^{235}U. The 4.2 K Mössbauer spectrum[26] of the ^{238}U 44.7 keV transition from the first excited state (2+) to the ground state (0+) in α-U yields a quadrupolar coupling constant, e^2qQ, of -2750±300 MHz. (No magnetic hyperfine fields greater than 300 kOe were detected.) Since the electric-field gradients experienced by ^{235}U and ^{238}U in α-U will be the same, using this value of e^2qQ and the A-value determined calorimetrically, assuming magnetic dipolar and impurity contributions are unimportant, a value of 1.6 is obtained for the ratio, Q_{235}/Q_{238}, for the nuclear electric-quadrupole moments of the ^{235}U ground state and of the ^{238}U first excited state.

2. The Electronic Heat Capacity

The γ-values determined in this study correlate with the grain size of the samples. The single crystal, Sample III, has the smallest γ-value, the large-grained Sample Ia has an intermediate γ-value, and the three remaining smaller grained samples exhibit larger γ-values of similar

magnitude to each other. This systematic variation is due to an increase in the degree of strain as the grain size is decreased, and it correlates with the observation that γ increased under pressure in one study[4] from 10.3 to 12.2 in mJ units between 0 and 10 kbar. Hence, in making comparisons with γ-values reported in the literature attention will be given to the metallurgical state of the sample. The γ-value of the single crystal coincides with the value 9.14 ± 0.29 mJ/K^2 mole recently determined for a pseudo single-crystal (approximately 10° mismatch between grains).[23] The γ-value of 9.86 mJ/K^2 mole for Sample Ib, the unannealed, swaged sample agrees with the value 9.88 ± 0.05 mJ/K^2 mole determined for another swaged sample that had been annealed in the α-phase, and hence was uniformly small grained.[27] The γ-values of 9.82 and 9.90 in mJ units found for Samples IIa and IIb, respectively, the pieces of U10, agree with the recently determined $\gamma=10.00\pm0.37$ mJ/K^2 mole for another piece[23] of U10, and agree somewhat less well with the value 10.3 obtained for the entire 74g U10 sample.[4] This latter disagreement of 4 and 5% with the earlier determination of γ is surprising since the temperature scale of the same laboratory was used in both experiments.

B. Superconducting-State Data

There are three published α-U heat capacity studies that extend below 1 K. One of these studies terminates at 0.65 K, hence it is likely that superconducting temperatures essentially were not reached.[28] In another study from approximately 0.4 K to 0.75 K it was impossible to tell whether or not the pure ^{235}U was superconducting, since C_N thoroughly dominated the heat capacity.[25] In this same study, natural U (0.7% ^{235}U) was examined between 0.17 K and 0.75 K, and it was concluded that superconductivity was absent. However, the coefficient of the T^{-2} term in the heat capacity was twice that expected from the ^{235}U content of the sample. Perhaps a broad superconducting transition was mistaken as an enhanced nuclear heat capacity. However the 600 Oe heat capacity data was indistinguishable from the zero-field results. Also, a very large γ-value of 12.1±0.3 mJ/K^2 mole was obtained. This presumably reflects systematic errors associated with the continuous heating technique employed to handle high activity samples, and with the temperature scale, which was based on an extrapolation of a carbon thermometer from above 1 K. Ho et al. examined four samples, and found an anomalous increase in C_E/T below 0.7 K in each case.[4] These anomalies were not attributed to superconductivity since one of the samples was found to be essentially field-independent in 2 kOe in a ^{3}He-cooled calorimeter, and in 2 and 5 kOe in an adiabatic demagnetization apparatus. Sample IIa and IIb are parts of the same sample studied in Ref. 4 at zero pressure and 10 kbar. It does not appear likely that the results of the earlier study can be reconciled with those of the current study based on models

assuming suppression, or partial suppression, of the 43 K volume-minimum in one case and not the other. Rapid liquid-helium quenches are necessary to suppress the volume minimum. In neither study did cooling proceed via direct contact with liquid-helium. There does not appear to be a satisfactory explanation of the lack of agreement between the two studies.

The shape of the superconducting-state heat capacity anomaly provides information on whether there is any 5f-localization as has been proposed[1] to occur at the 43 K anomaly, and to be responsible for the low-pressure depression in T_c relative to the 10 kbar maximum of approximately 2 K. Considering Sample Ia, the maximum difference between C_{En} and C_{Es} at the broadened transition occurs at approximately 0.24 K. This temperature corresponds to a T_c that is 12% of its 2 K value. In the BCS theory this would correspond to a heat capacity jump only 12% of its T_c=2 K value of 1.43 γT_c, and in the AG theory to 3% of its 2 K value.[29] Experimentally the jump at 0.24 K is 6.5% of its 10 kbar value. (This is clearly a lower limit since the jump is smeared.) Hence the depression in T_c is not governed by the AG theory--pair-breaking mechanisms and local moments do not play a role in the properties of α-U. This conclusion is consistent with the neutron diffraction and magnetic susceptibility results.[10,11]

The superconducting transitions shown in Fig. 2-4 are broad, and it is not clear that they will be complete by 0 K. Broadened BCS heat capacity curves were used to represent the data in order to determine if a non-zero (C_E/T)-value would persist to 0 K, corresponding to a fraction of the sample remaining in the normal state. Assuming that strain produces a distribution, $f(T_c)$, of T_c-values, at temperature T, the total electronic heat capacity consists of a contribution from the

fraction of the material in the superconducting state, and the fraction in the normal state:

$$C_E(T)=\int_T^\infty f(T_c)C_{Es}(T_c,T)dT_c+\int_o^T f(T_c)C_{En}(T)dT_c \qquad (2)$$

Bucher, et al. used a similar approach to characterize the broadened superconducting transitions of some titanium alloys.[30] Values of $C_{Es}(T_c,T)$ can be obtained from published tables of the thermodynamic functions of BCS superconductors.[31a] Using a normalized Gaussian distribution where the mean T_c is $\bar{T}_c$, and the half-width of the transition is δT_c, $C_E(T)$ can be obtained by numerical integration of the right-hand side of Eq. 2. Curves corresponding to the calculated $C_E(T)/T$-values for values of $\bar{T}_c$ and δT_c which fit the data reasonably well are plotted in Figs.2 through 4, and the corresponding $\bar{T}_c$ and δT_c values appear in Table III. The calculated curves are plotted together in Fig. 7 as $C_E/\gamma T$ vs. T. From the T=0 K intercepts the molefraction of sample in the superconducting state at T=0 K, n_{Es}, was obtained in each case, and collected in Table III.

Sample Ia appears to be totally superconducting by 0 K. For Samples Ib and II this appears not to be the case, however, these n_{Es}-values were sensitive to small variations in $\bar{T}_c$ and δT_c, as was not the case for Sample Ia. For Sample II, n_{Es} is close enough to 1 that it is quite plausible that n_{Es} is equal to 1. For Sample Ib the situation is ambiguous, since the data can be fit to a distribution function with $\bar{T}_c$=0 K and δT_c=0.42 K, for which n_{Es}=0.9 when $f(T_c)$ is normalized by the factor 1.8. This gives an indication of the limited sensitivity of the approach.

Low-temperature resistivity investigations of the multiplicity of α-phases in uranium below 43 K indicate that within 30 to 45 minutes after intermediate-metastable α-phases are quenched-in, uranium transforms to its single equilibrium phase.[16] For all samples in this study the temperature was less than 4.2 K for several hours before heat capacity data were obtained. Obviously then these samples were in their single equilibrium phase were the measurements were made.

Ho et al. concluded that the pressure dependence of T_c cannot be fully accounted for by the pressure dependence[4] of the electronic density-of-states as reflected in the γ-value. This remains so even though the γ-value of single-crystal α-U at zero pressure is significantly lower than that of the polycrystal the conclusion was based upon. A reduction in Coulombic repulsion with increasing pressure associated with the changing nature of the *f*-electrons might account for the balance of the pressure-enhancement in T_c.

Uranium metal belongs to the group of actinides, Th to Am, whose properties are intermediate between those of the corresponding rare-earth and 5d-transition metals.[31b] The 5*f*-electrons of U are less localized than are the 4*f*-electrons of the rare-earth metals, but they are more localized than are the 5d-electrons of the third transition series. The 5*f*-electrons, therefore, are expected to contribute correspondingly less to the cohesive energy of the metal and to the determination of long-range order than the 5d-electrons. The narrow 5*f*-bands in U metal broaden due to hybridization with s-, p-, and d-electron states. Pressure further broadens these 5*f*-like hybrid

bands enhancing f-contribution to cohesion and reducing Coulombic repulsion, the source of pair-weakening. It has been documented that pair-weakening effects can depress T_c as dramatically as local moments.[32]

The large deviation from the BCS isotope effect[5] for α-U at 11 kbar indicates that at this pressure Coulombic repulsion is still quite important. However at higher pressures T_c decreases. Maple found that at approximately 90 kbar, T_c is approximately 0.4 K.[33] The behavior of the density of states is not known above 10 kbar. However, it has been conjectured that for α-U the electron-phonon interaction strength itself may be pressure sensitive, based on the pressure sensitivity of the phonon spectrum of dhcp La found in recent superconducting tunneling experiments.[34] Further experimental work is necessary to test this.

The role of f-electrons in superconductivity has been the subject of considerable interest and debate.[35] This also applies to the nature of the f-character itself, as reflected, for instance, in the complex crystal structures found in the earlier 5f-electron elements. Complex structures appear when there are two or more electronic configurations of comparable stability available.[36] Crystallographically inequivalent sites can then assume different configurations, have varied radii, and pack more densely than close-packed structures. Pauling proposed this to describe the α- and β-Mn structures.[37] γ-U, stable below the liquid phase, is bcc, and hence, is characterized by a single electronic configuration. Based on studies of stabilized γ-U alloys containing approximately 20 at. % Mo and Nb, a normal BCS isotope effect was found, and a hypothetical T_c-value for pure γ-U was estimated to be

2.1 K.[38] The isotope-effect result may mean that the electronic configuration of γ-U contains no significant *f*-contributions or that the *f* electrons behave like the other itinerant electrons. The T_c-value corresponds approximately to the maximum T_c of α-U. In β-U, a complex structure, there are large size differences on inequivalent sites. (Intermetallics crystallize in the β-U-structure only when there are large atomic-size differences.) The superconducting transitions of 1.75 at.% Pt- and Cr- stabilized β-U are sharp, BCS-like, and occur at 0.85 K and 0.75 K, respectively.[39] As in α-U, pair-weakening effects due to narrow *f*-like hybridized bands are expected in β-U, as are deviations from the BCS isotope effect. Isotope effect information for stabilized β-U alloys, however is lacking.

REFERENCES

1. T. H. Geballe, B. T. Matthias, K. Andres, E. S. Fisher, T. F. Smith and W. H. Zachariasen, Science 152, 755 (1966).

2. C. Palmy and E. S. Fisher, Solid State Comm. 8, 653 (1970).

3. E. S. Fisher, T. H. Geballe and J. M. Schreyer, J. Appl. Phys. 39, 4478 (1968).

4. J. C. Ho, N. E. Phillips and T. F. Smith, Phys. Rev. Lett. 17, 694 (1966); also reported in Proceedings of the Tenth International Conference on Low Temperature Physics, edited by N. V. Zavaritsky and I. P. Krylov (Moscow, 1967) Vol. IIb, p. 189.

5. R. D. Fowler, J. D. G. Lindsay, R. W. White, H. H. Hill, and B. T. Matthias, Phys. Rev. Lett. 19, 892 (1967).

6. A. F. Shuck and H. L. Laquer, Phys. Rev. 86, 803 (1952).

7. E. S. Fisher and H. J. McSkimin, Phys. Rev. 124, 67 (1961).

8. E. S. Fisher and D. Dever, Phys. Rev. 170, 607 (1968).

9. C. S. Barrett, M. H. Mueller and R. L. Hitterman, Phys. Rev. 129, 625 (1963).

10. G. H. Lander and M. H. Mueller, Acta Cryst. B26, 129 (1970).

11. J. W. Ross and D. J. Lam, Phys. Rev. 165, 617 (1968).

12. T. G. Berlincourt, Phys. Rev. 114, 969, (1959).

13. A. Hough, J. A. C. Marples, M. J. Mortimer and J. A. Lee, Phys. Lett. 27A, 222 (1968).

14. K. Andres, Phys. Rev. 170, 614 (1968).

15. M. B. Brodsky, N. J. Griffin and M. D. Odie, J. Appl. Phys. 40, 895 (1969).

16. N. H. Sze and G. T. Meaden, Plutonium 1970 and Other Actinides, edited by W. N. Miner (Metallurgical Soc. AIME, New York, 1970) TMS Nuclear Metallurgy Series Vol. 17, p. 974.

17. J. A. C. Marples, J. Phys. Chem. Solids, 31, 2421 (1970).

18. E. S. Fisher and D. Dever, Solid State Commun. 8, 649 (1970).

REFERENCES - page 2

19. W. E. Gardner and T. F. Smith, Phys. Rev. 154, 309 (1967).

20. M. O. Steinitz, C. E. Burleson and J. A. Marcus, J. Appl. Phys. 41, 5057 (1970).

21. M. Rosen, Phys. Lett. 28A, 438 (1968).

22. T. F. Smith and E. S. Fisher, J. Low Temp. Phys. 12, 631 (1973).

23. J. Crangle and J. Temporal, J. Phys. F: Metal Phys., 3, 1097 (1973).

24. E. S. Fisher, Trans. AIME 209, 882 (1957).

25. C. W. Dempesy, J. E. Gordon, and R. H. Romer, Phys. Rev. Lett. 11, 547 (1963).

26. S. L. Ruby, G. M. Kalvius, B. D. Dunlap, G. K. Shensy, D. Cohen, M. B. Brodsky, and D. J. Lam, Phys. Rev. 184, 374 (1969).

27. H. E. Flotow and D. W. Osborne, Phys. Rev. 151, 564 (1966).

28. J. E. Gordon, H. Montgomery, R. J. Noer, G. R. Pickett, and R. Tobón, Phys. Rev. 152, 432 (1966).

29. S. Skalski, O. Betbeder-Matibet, and P. R. Weiss, Phys. Rev. 136, A1500 (1964).

30. E. Bucher, F. Heiniger, and J. Muller, Proceedings of the Ninth International Conference on Low Temperature Physics, edited by Daunt, et al., (Columbus, Ohio, 1965) p. 482.

31a. B. Mühlschlegel, Z. Physik 155, 313 (1959).

31b. See, for instance: R. Jullien, E. Galleani d'Aglino, and B. Coqblin, Phys. Rev. B6, 2139 (1972).

32. See, for instance: M. B. Maple, in Superconductivity in d- and f-band Metals, AIP Conference Proceedings No. 4, edited by D. H. Douglass (AIP, New YOrk, 1972) p. 175.

33. See T. F. Smith, ibid. p. 293.

34. H. Wühl, A. Eichler and J. Wittig, Phys. Rev. Lett. 31, 1393 (1973).

35. See, for instance: J. W. Garland, Naval Research Laboratory Report No. 6962 (1969) unpublished; and J. Appel, Phys. Rev. B8, 1079 (1973).

REFERENCES - page 3

36. L. Brewer, Science 161, 115 (1968).

37. L. Pauling, J. Am. Chem. Soc. 69, 542 (1947).

38. H. H. Hill, R. W. White, J. D. G. Lindsay, R. D. Fowler and B. T. Matthias, Phys. Rev. 163, 356 (1967).

39. B. T. Matthias, T. H. Geballe, E. Corenzwit, K. Andres, G. W. Hull, Jr., J. C. Ho, N. E. Phillips, and D. K. Wohlleben, Science 151, 985 (1966).

Table I. Description of the Samples

Sample	at.% ^{235}U	at.% ^{234}U	Weight	Physical Form	Magnetic Transition
Ia	0.16	0.001	9.599g	Large-grained polycrystal; 1/8 inch diameter	0.3-0.45K[a]
Ib			8.023g	Striated, cold worked structure; 1/16 inch diameter	0.9-1.4 K[a]
IIa	0.23	-	11.568g	Strain-annealed polycrystal; heavily electro-etched	0.6-0.9 K[b]
IIb			11.048g	Strain-annealed polycrystal; unetched.	
III	0.4043	0.00266	1.848g	Grain-coarsened single crystal	0.2-0.45K[c]

a) See Ref. 3
b) See Ref. 22
c) This work

Table II. Summary of α-U Heat Capacity Measurements.

Sample	Field (Oe)	Temperature Interval (K)
Ia	0	0.15 - 2.1
Ia	50	0.16 - 1.1
Ia	100	0.15 - 1.0
Ib	0	0.21 - 2.1
Ib	500	0.31 - 2.0
IIa	0	0.17 - 1.8
IIa	500	0.18 - 2.2
IIb	0	0.18 - 0.9
IIb	500	0.22 - 2.1
III	0	0.13 - 1.3
III	200	0.10 - 2.2

Table III. Calorimetrically determined properties of α-U.

Sample	A (mJ-K/mole ^{235}U)	γ (mJ/K^2mole)	Onset T_c (K)	$\bar{T}_c$(K)	δT_c(K)	n_{Es}
Ia	- -	9.59	0.4	0.27	0.05	1.0
Ib	- -	9.86	> 1.0	0.20	0.35	0.7
IIa	10.3	9.82	0.7	0.27	0.20	0.9
IIb	10.7	9.90				
III	11.4	9.14	(0.25)	-	-	-

FIGURE CAPTIONS

Fig. 1. The heat capacity of Sample III in 200 Oe and Sample IIa in 500 Oe plotted as CT^2 vs T^3. The straight lines represent the least-squares fitted values of the nuclear and electronic heat capacity contributions plotted as $fA + \gamma T^3$ vs T^3.

Fig. 2. The electronic heat capacity of Sample Ia. The horizontal line represents the γ-value. The curve represents a BCS heat capacity anomaly broadened by a Gaussian distribution of transition temperatures, with $\bar{T}_c = 0.27$ K and $\delta T_c = 0.05$ K.

Fig. 3. The electronic heat capacity of Sample Ib. The horizontal line represents the γ-value. The curve represents a BCS heat capacity anomaly broadened by a Gaussian distribution of transition temperatures, with $\bar{T}_c = 0.2$ K and $\delta T_c = 0.35$ K.

Fig. 4. The electronic heat capacity of Sample IIa and Sample IIb. The horizontal line represents the γ-value of Sample IIa. The curve represents a BCS heat capacity anomaly broadened by a Gaussian distribution of transition temperatures, with $\bar{T}_c = 0.27$ K and $\delta T_c = 0.2$ K.

Fig. 5. The electronic heat capacity of Sample III. The horizontal line represents the γ-value.

Fig. 6. The superconducting transition of Sample III detected magnetically.

Fig. 7. The calculated electronic heat capacities appearing in Figs. 2 through 4 plotted as $C_E/\gamma T$ vs T. The T = 0 K intercepts indicate that n_{Es} is 1, 0.9 and 0.7 for Samples Ia, IIa and Ib, respectively.

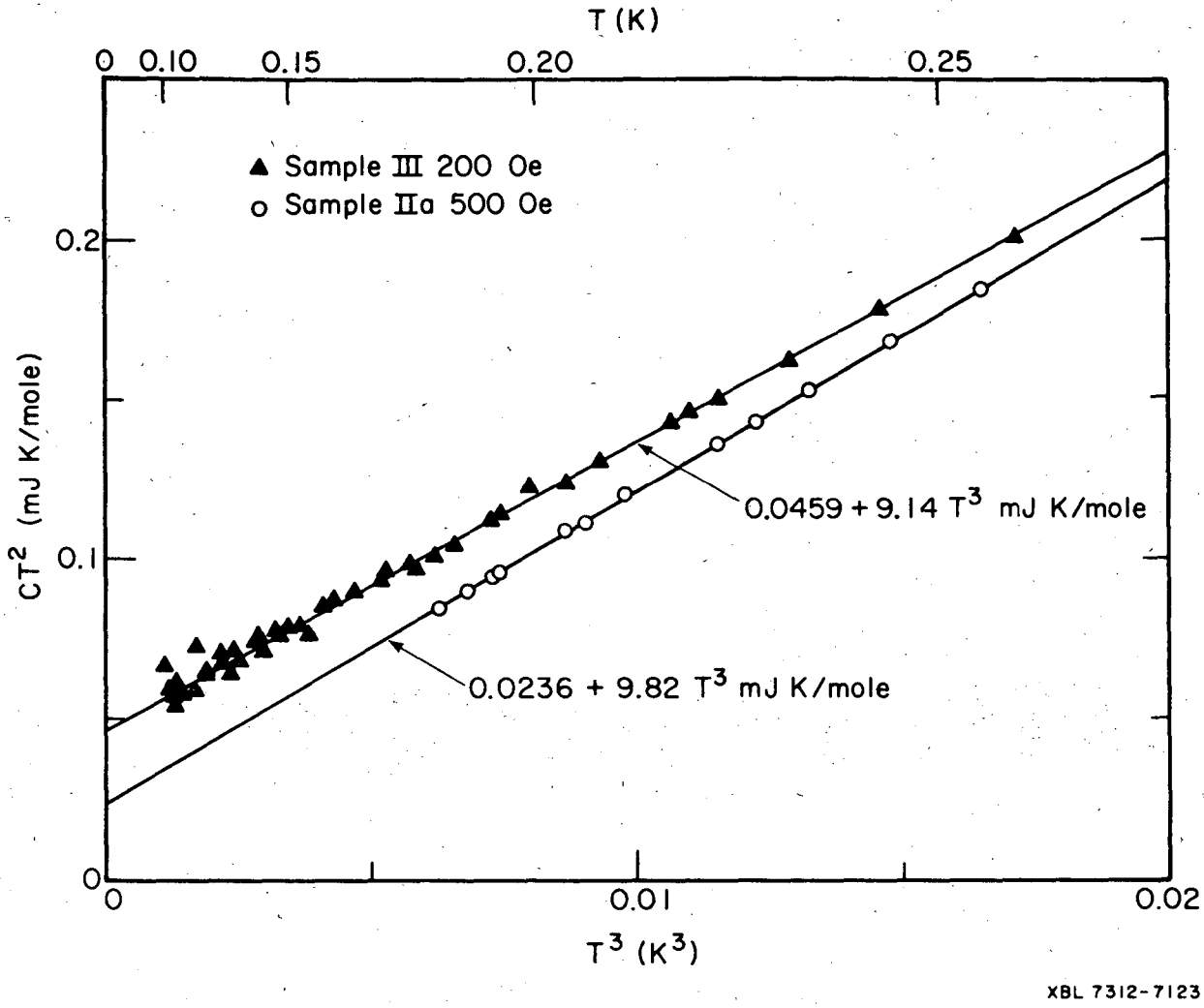
T (K)
0
0.10
0.15
0.20
0.25
▲ Sample III 200 Oe
o Sample IIa 500 Oe
0.2
0.1
0
CT^2 (mJ K/mole)
0.0459 + 9.14 T^3 mJ K/mole
0.0236 + 9.82 T^3 mJ K/mole
0
0.01
0.02
T^3 (K^3)
XBL 7312-7123

Fig. II-1.

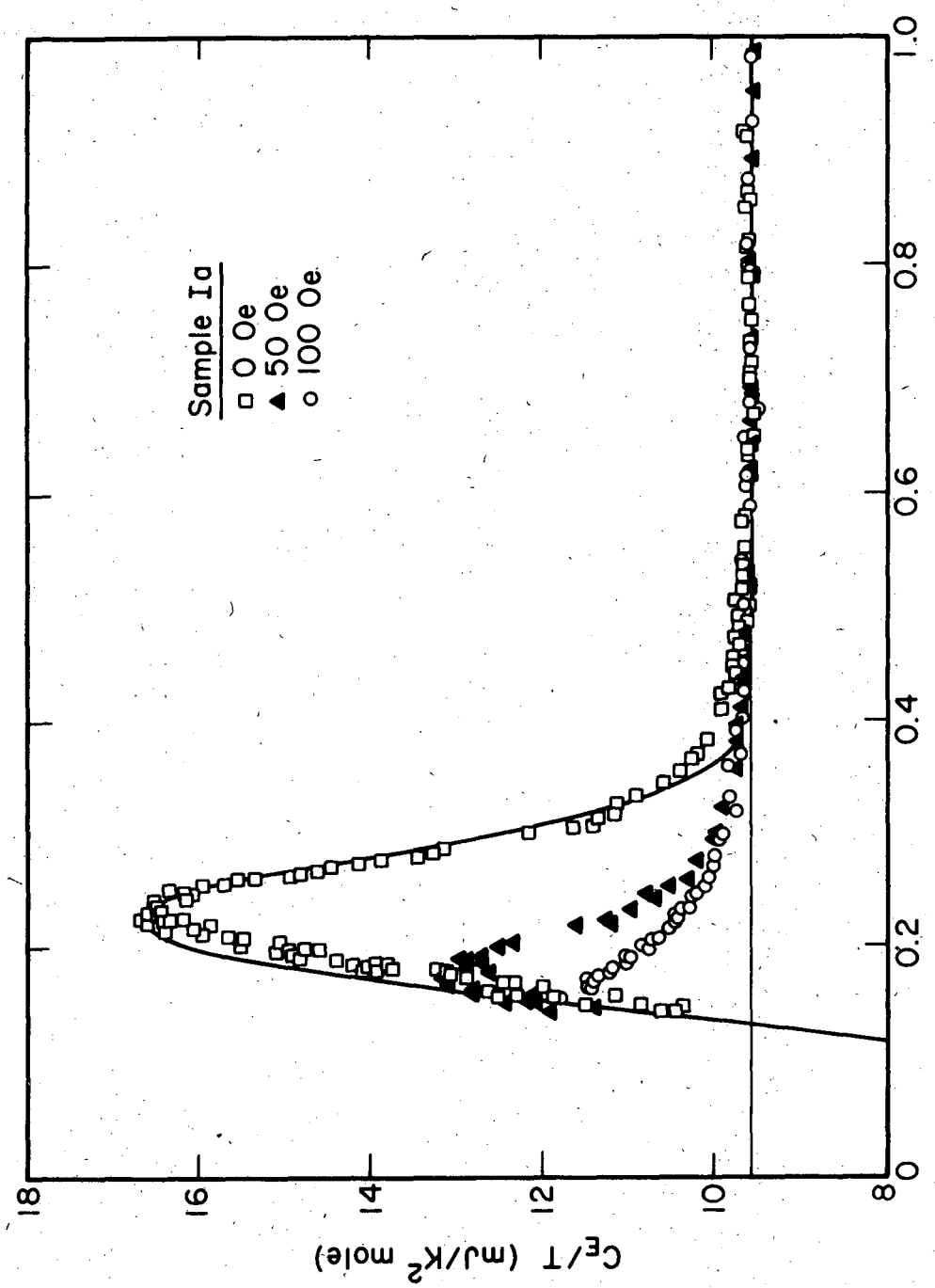

XBL 7312-7125

Fig. II-2.

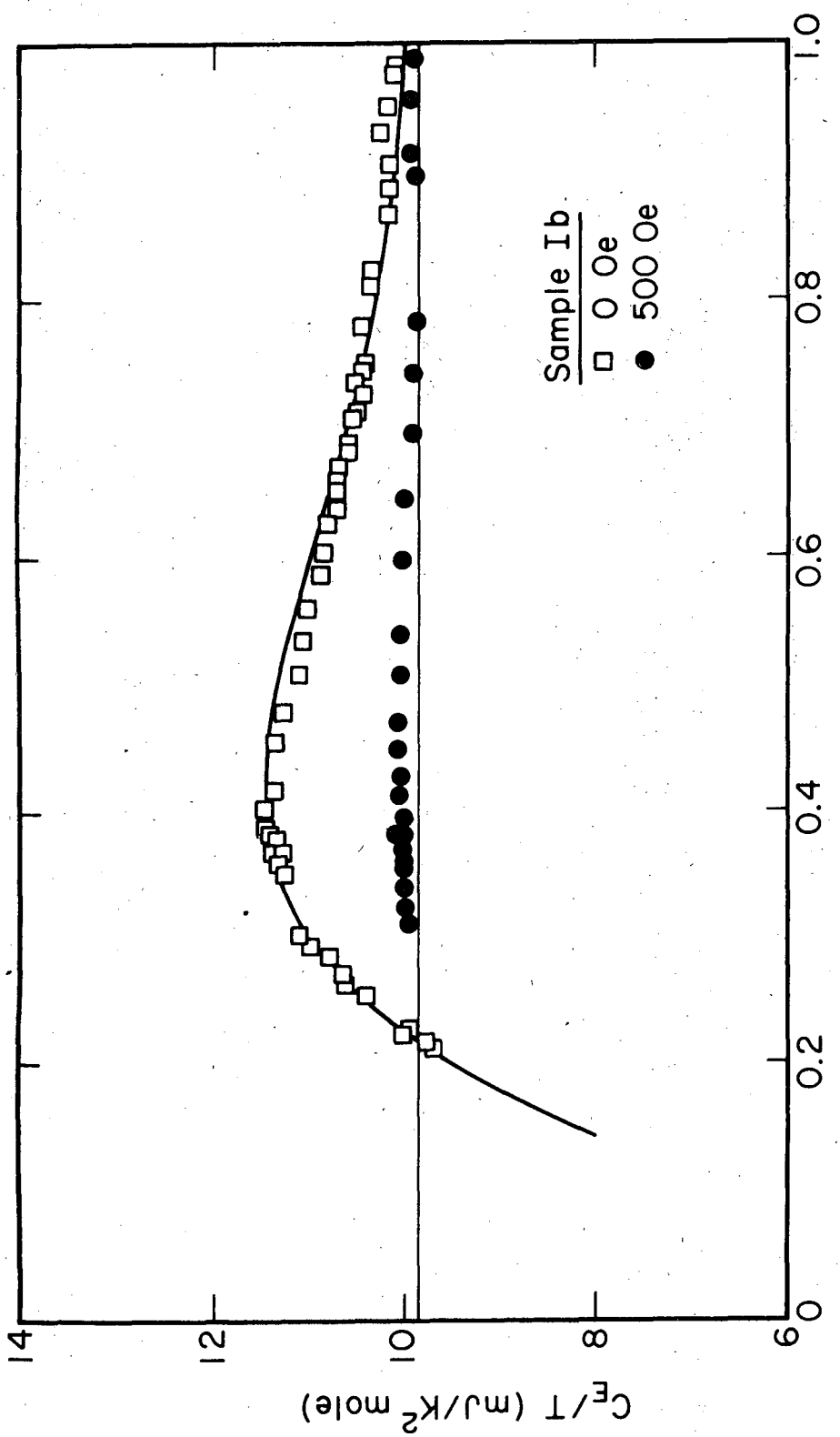

XBL 7312-7124

Fig. II-3.

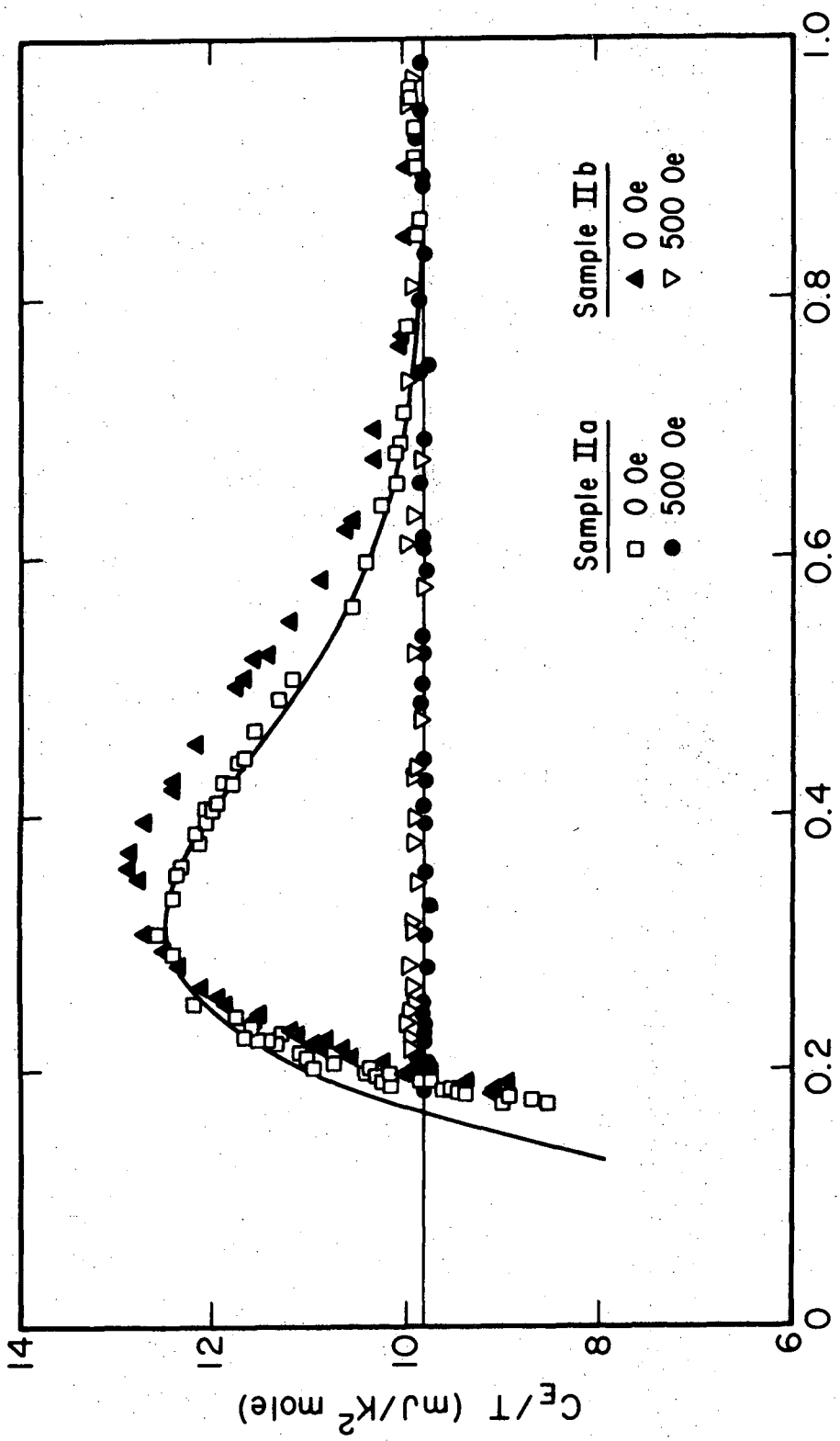
C_E/T (mJ/K^2 mole)
T (K)
Sample IIa
0 Oe
500 Oe
Sample IIb
0 Oe
500 Oe
XBL 7312-7129

Fig. II-4.

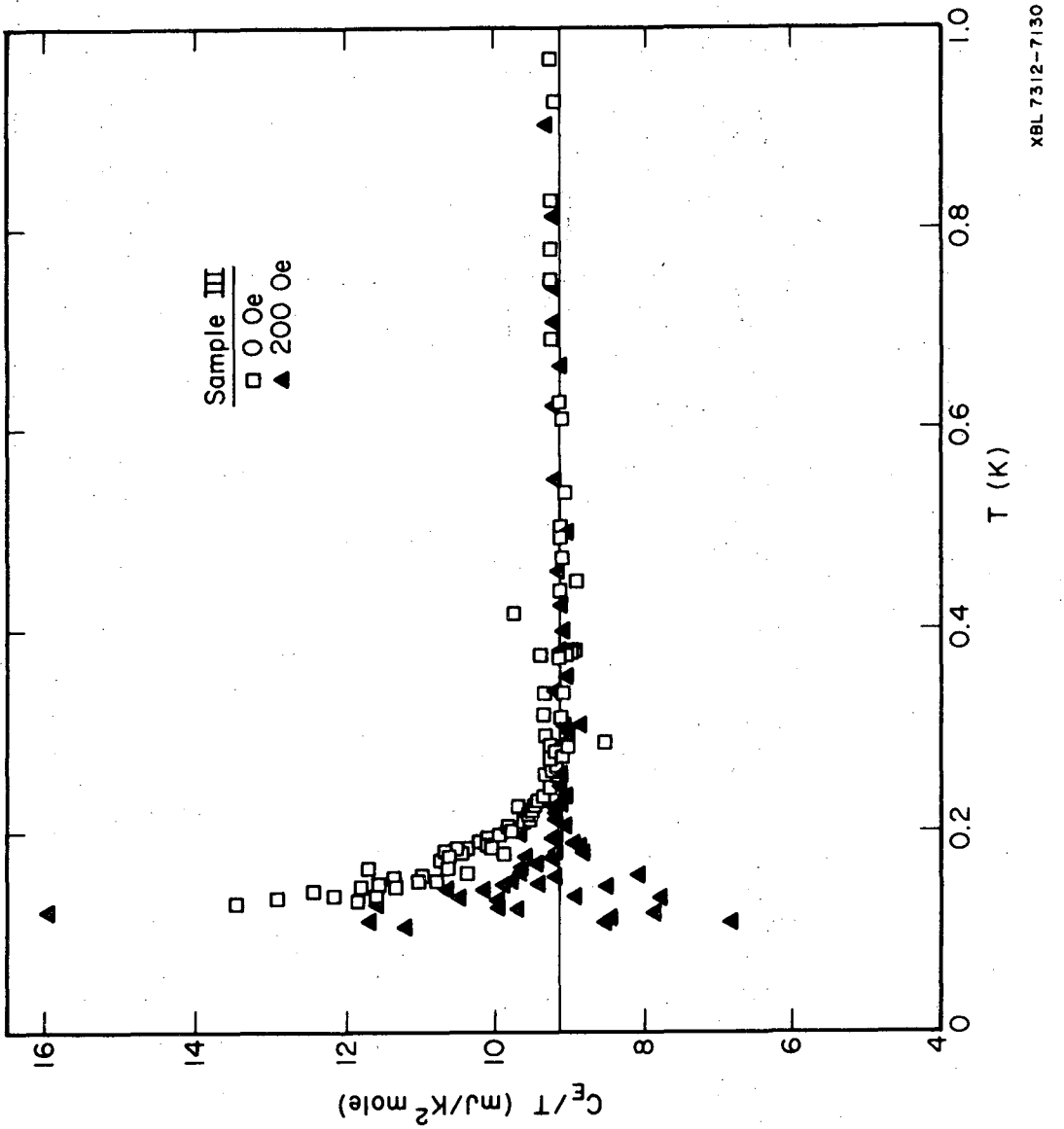
Sample III
0 Oe
200 Oe
C_E/T (mJ/K^2 mole)
T (K)
16
14
12
10
8
6
4
0
0.2
0.4
0.6
0.8
1.0
XBL 7312-7130

Fig. II-5.

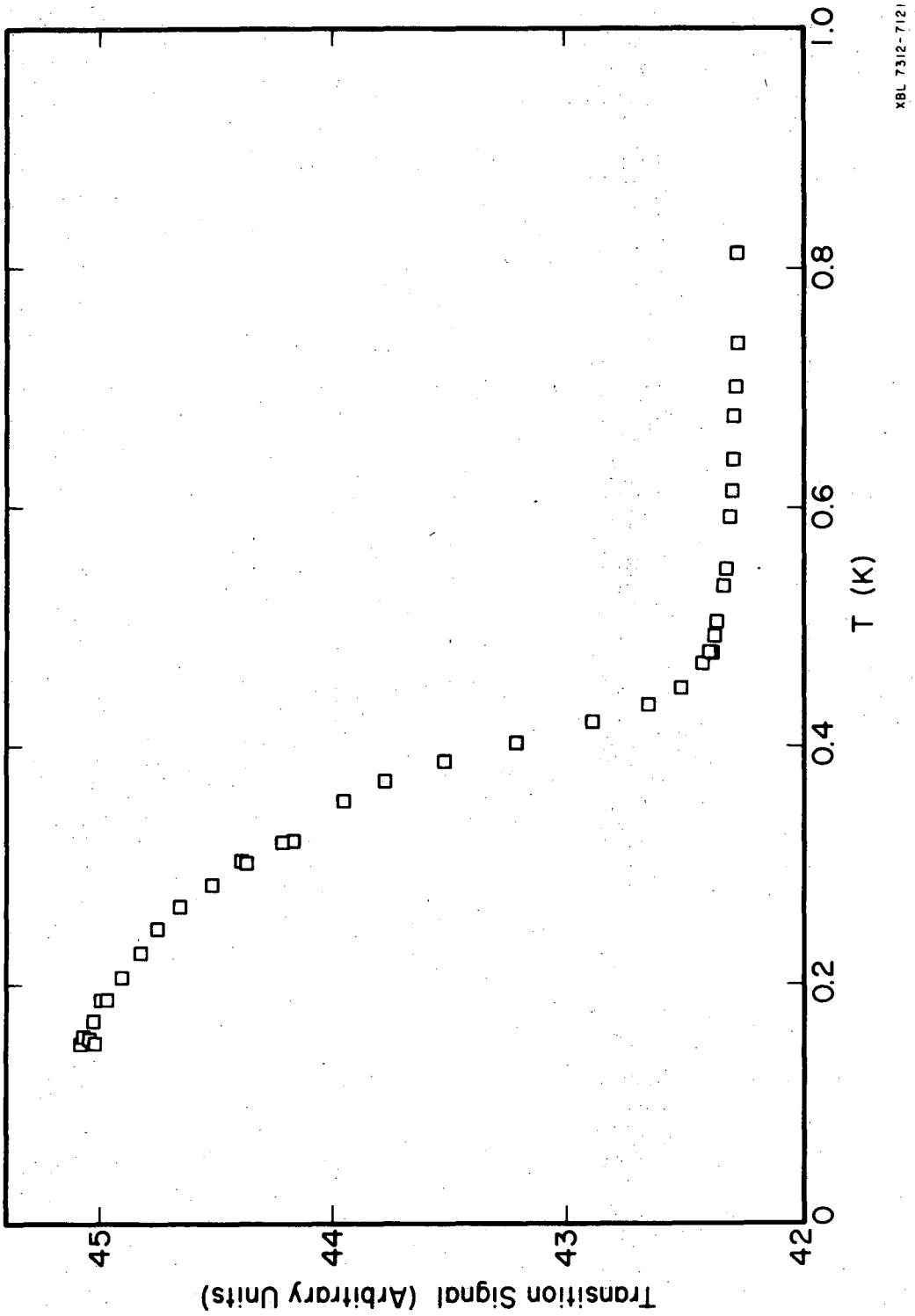
Transition Signal (Arbitrary Units)
45
44
43
42
0
0.2
0.4
0.6
0.8
1.0
T (K)
XBL 7312-7121

Fig. II-6.

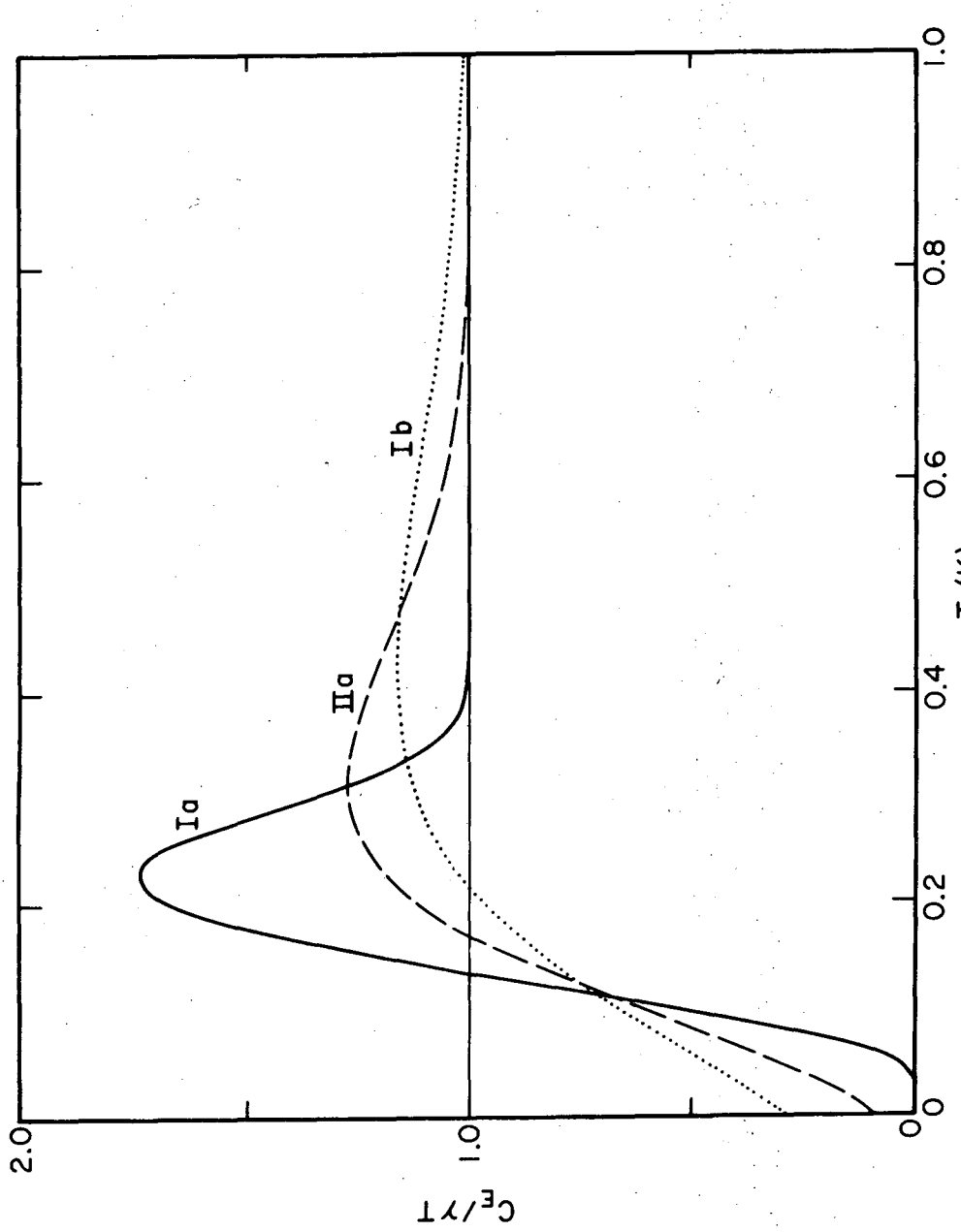

Fig. II-7.

PART THREE: SmS

An unusual class of materials that contain rare earth ions with nonintegral valence and "soft" magnetic moments has recently been recognized.[1] Samarium sulfide exhibits the properties characteristic of these materials at pressures above 6.5 kbar but not at lower pressures and is, therefore, a particularly interesting system for further study.[2] The first order metal-insulator transition at 6.5 kbar and 298 K in SmS is marked by an 8% decrease in volume with no change in crystal structure.[3] There is a factor of 10 increase in optical reflectivity[4] at 0.8μ but only a factor of five decrease in resistivity at the transition. In addition, the resistivity was found to increase with decreasing temperature in the metallic phase.[5] At 10 and 20 kbar the resistivity is approximately 200 μΩcm at room temperature, however, at 3 K the resistivity is approximately 1200 and 700 μΩcm, respectively.[5] The change in resistivity[5] at the transition is 10^4 greater at 4.2 than at 473 K. At the transition at room temperature the magnetic susceptibility decreases by 60%, and no evidence for magnetic ordering was found down to 1 K.[2] It has been proposed that there is a partial electronic rearrangement at the transition from an insulating phase in which Sm^{+2} ions are in the non-magnetic ^7F_o ground state of the $4f^6$ configuration to a metallic phase in which, in time average, 0.7 electrons are transferred to a conduction band.[2] To account for the observed susceptibility, it was suggested that the $4f$ levels form virtual bound states tied to the Fermi energy.[2] These effects are also

observed[6,7] in SmB_6. In fact, the features of the heat capacity and resistivity are similar in the two materials which supports the suggestion[2] that a common model must be used to explain the unusual properties.

The heat capacity measurements were made in a ^3He cryostat by a heat pulse method using germanium thermometers which give a precision from experiment to experiment of approximately 0.1%. For the measurements in the metallic phase a piston and cylinder device was used in which pressure is applied at room temperature in a conventional press and then retained by a mechanical clamp. The cell is shown schematically in Fig. 1. By comparison with strain-gauge measurements on similar cells, it was estimated that as much as 80 to 90% of the load could be retained by the locking nut at room temperature.[8] The thermal expansions of the cell materials suggest there should be no further pressure loss on cooling. The same cell was used to study the heat capacity of V_2O_3 at high pressure.[9] In order to achieve higher pressures than in earlier cerium[10] and uranium[11] experiments, the body of the cell was made of hardened Berylco 25 and the mushroom-shaped piston was made of tungsten carbide.[12,13] The cell was prestretched to 28 kbar using a tungsten carbide end plug and a soft copper sample and then the inside diameter was bored to a uniform radius. (A single insulated electrical lead was added using a conventional cone seal, so that resistance measurements could be monitored.)

The heat capacity of the empty cell was determined at 1 and at 25 kbar by measuring the heat capacity of the cell filled with pure diamond powder, which has a negligible heat capacity compared with that of the cell.[14] The heat capacity of the cell is shown as the deviation from

$$C_C \equiv A_o + \sum_{i=-1}^{4} A_{2i+1} T^{2i+1} \qquad (1)$$

in Fig. 2. The coefficients[15] in Eq. (1) were obtained by a least squares fit to the 1 kbar data, and the heat capacity of the cell could be represented by Eq. (1) and tables that correspond to the appropriate curve in Fig. 2. A 4.12g sample of SmS, which comprised 1.58% of the total weight of the cell and sample, was compressed and the transition monitored by the advance of the piston. After applying 20 kbar load load to the cell, the locking nut was tightened, and an estimated 15 kbar pressure was retained on the sample. For the calculation of the heat capacity of the metallic SmS, the heat capacity of the cell as calculated from Eq. (1) was corrected by a factor found by interpolation in the 25 kbar table. (The weak pressure-sensitivity of the cell heat capacity could cause systematic errors in the high-pressure SmS results of less than 1%.)

The results of the heat capacity measurements of SmS at zero pressure and at approximately 15 kbar from 0.3 to 20 K are shown in Fig. 3. The large heat capacity of the metallic phase relative to the insulating phase is evident. A plot of C/T vs T^2 shows that the limiting coefficient of the linear term in the heat capacity of the

metallic phase is $\gamma \approx 145$ mJ/mole K^2. (Use of the symbol γ is not intended to imply that this heat capacity is an ordinary conduction electron contribution that can be extrapolated to high temperatures--such an extrapolation would give a very high room-temperature heat capacity.) A small anomaly that occurs near 3 K at zero pressure and at 15 kbar is probably associated with impurities. (Such effects have frequently been observed in rare earths and their compounds.) At zero pressure the anomalous region is shown more clearly in Fig. 4 in 0 and 38 kOe. Although at 15 kbar the anomaly occurs at a somewhat higher temperature than at zero pressure, as expected, (See Fig. 3). At 0 pressure the anomaly is remarkably field insensitive. In 38 kOe a second anomaly can be identified in Fig. 4 below 1 K. This lower-temperature anomaly can be attributed to the ordering of a impurity electronic moment with a very small g-factor, or to an enhanced nuclear hyperfine field due to the polarization of an impurity singlet electronic ground state in the external field. Spark-source mass-spectroscopic analysis indicated that the SmS contained approximately 100 ppm T_m and 100 ppm Er. Thulium usually has a singlet ground state. The 0 kOe anomaly obscures any linear term in the zero-pressure heat capacity. But an upper limit of approximately 7 mJ/mole K^2 can be assigned for the value of γ in the insulating phase, based on a least-squares fit of the data between 5 K and 10 K to the expression:

$$C = AT^{-2} + \gamma T + B_3 T^3 + B_5 T^5 \ . \qquad (2)$$

The lattice parameters of metallic SmS and SmB_6 suggest that the relative contributions of the $4f^5$ and $4f^6$ configurations are in the ratio 7:3.[1,2] (The isomer shift[16] and energy of the L_{III} X-ray absorption edge[17] have also been measured for SmB_6, and indicate the same ratio.) The lowest term for the $4f^5$ configuration is $^6H_{5/2}$ and in an octahedral field this term splits into a Γ_7 doublet and a Γ_8 quartet level. Inelastic neutron scattering experiments on PrS show that the Γ_7 doublet lies lowest, and a Γ_7-Γ_8 separation of 165 K is obtained for SmS by scaling the PrS results as the fifth power of the lattice parameter.[18] The Rℓn2 entropy of the Γ_7 Kramer's doublet must disappear as $T \to 0$, and this usually occurs through magnetic ordering as in, for example, CeB_6[19] and $CePb_3$.[20] Integration of C/T for both the metallic and insulating phases of SmS as a function of temperature shows that the entropy change at the transition, $\Delta S = S_{metal} - S_{insulator}$, increases smoothly from 0 at 0 K to 0.54 R at 20 K. This is close to 0.7 Rℓn2 which suggests that the Γ_7 doublet in metallic SmS loses its entropy gradually, and in a temperature interval in which susceptibility measurements show no indication of magnetic ordering.

Using the slope of the phase boundary[5] $dT/dP \sim -200$ K/kbar, the entropy change at 298 K is calculated from the Clapeyron equation to be $(0.15 \pm 0.1)R$, substantially smaller than ΔS_{20}. The initial rapid increase in ΔS is balanced at higher temperatures by other factors such as population of higher energy levels in the $4f^5$ and $4f^6$ multiplets and different Debye temperatures. Plausible values

would be 165 K for the Γ_7-Γ_8 splitting,[18] 415 K for the $^7F_0$-$^7F_1$ splitting[21] of the $4f^6$ configuration, γ = 8 mJ/mole K^2 for the conduction electrons, 266 K for the Debye temperature at zero pressure based on the B_3 coefficient in Eq. (2), and a Grüneisen parameter of 1.5. Such a model would give ΔS_{298} = 0.2 R which is similar to the observed value of (0.15 ± 0.1) R. In Fig. 5 the entropy contributions are plotted through room temperature using these parametric values, as are the experimental determinations of the entropy change up to 20 K and at room temperature. (The calculation of the high-pressure Debye temperature is, of course, only a crude approximation, but, for example, a change of 0.5 in the effective Grüneisen parameter changes the calculated ΔS_{298} by 0.1 R, which comparable to the uncertainties in the experimental ΔS_{298} and in the other terms in the calculated ΔS_{298}.)

The unusual properties exhibited by metallic SmS and SmB_6, and which would have to be explained by a successful microscopic theory, are: 1) the absence of magnetic ordering and the saturation of the magnetic susceptibility at low temperatures, 2) the apparent intermediate electronic configuration of 0.7 f^5 and 0.3 f^6 derived from volume considerations, 3) the large linear term in the heat capacity and the continuous demagnetization of the 4f electrons, and 4) the large rise in resistivity below 50 K. It has been suggested[2] that α-Ce also belongs in this group of materials, and $CeSn_3$ and $CeBe_{13}$ are possible additional examples--both have the Γ_7 crystal field ground state, large linear terms in the low-temperature heat capacity, and

susceptibilities that saturate at low temperatures with no indication of a divergence or magnetic ordering.[20]

REFERENCES

1. See, for instance, D. Wohlleben and B. Coles, in Magnetism: A Treatise on Modern Theory and Materials, edited by H. Suhl (Academic Press, New York, 1973) Vol. 5.
2. M. B. Maple and D. Wohlleben, Phys. Rev. Lett. 27, 511 (1971).
3. A. Jayaraman, V. Narayanamurti, E. Bucher, and R. G. Maines, Phys. Rev. Lett. 25, 1430 (1970).
4. J. L. Kirk, K. Vedam, V. Narayanamurti, A. Jayaraman, and E. Bucher, Phys. Rev. B 6, 3023 (1972).
5. S. D. Bader, N. E. Phillips, and D. B. McWhan, Phys. Rev. B 7, 4686 (1973).
6. A. Menth, E. Buehler, and T. H. Geballe, Phys. Rev. Lett. 22, 295 (1969).
7. J. C. Nickerson, R. M. White, K. N. Lee, R. Bachmann, T. H. Geballe, and G. W. Hull, Jr., Phys. Rev. B3, 2030 (1971).
8. T. F. Smith and H. L. Luo, J. Phys. Chem. Solids 28, 569 (1967).
9. D. B. McWhan, J. P. Remeika, S. D. Bader, B. B. Triplett and N. E. Phillips, Phys. Rev. B 7, 3079 (1973).
10. N. E. Phillips, J. C. Ho and T. F. Smith, Phys. Letters 27A, 49 (1968).
11. N. E. Phillips, J. C. Ho and T. F. Smith, Phys. Rev. Letters 17, 694 (1967).
12. Kawecki-Berylco Industries, P.O. Box 1462, Reading, Pa. 19603.
13. W. Paul, G. B. Benedek and D. M. Warschauer, Rev. Sci. Inst. 30, 874 (1959).

14. We are grateful to H. Tracy Hall, Jr., for suggesting the use of powdered diamond.

15. The approximate values of the coefficients are $A_{-1} = 0.450$, $A_o = 0.552$, $A_1 = 3.44$, $A_3 = 0.185$, $A_5 = 6.13\times10^{-5}$, $A_7 = 2.42\times10^{-7}$, and $A_9 = -3.09\times10^{-10}$, in mJ units. The T^{-1} and T^0 terms are very probably associated with the 241g of beryllium copper in the cell. Heat capacity measurements on two other Berylco 25 samples (J. C. Ho and N. E. Phillips, unpublished) have shown T^{-1} and T^0 terms of similar magnitude but differing from each other by approximately a factor of two.

16. R. L. Cohen, M. Eibschütz, and K. W. West, Phys. Rev. Lett. 24, 383 (1970).

17. E. E. Vainshtein, S. M. Blokhin, and Yu. B. Paderno, Fiz. Tverd. Tela 6, 2909 (1964). [Soviet Phys. Solid State 6, 2318 (1965)].

18. We are indebted to R. J. Birgeneau for calculating the Γ_7-Γ_8 splitting. The experimental value for PrS was reported by K. C. Turberfield, L. Passell, R. J. Birgeneau and E. Bucher, J. Appl. Phys. 42, 1746 (1971).

19. K. N. Lee and B. Bell, Phys. Rev. B6, 1032 (1972).

20. J. R. Cooper, C. Rizzuto and G. Olcese, J. Phys. (Paris) 32, C1-1136 (1971).

21. W. E. Bron and W. R. Heller, Phys. Rev. 136A, 1433 (1964).

FIGURE CAPTIONS

Fig. 1. Schematic drawing of the high-pressure heat-capacity cell and related parts.

Fig. 2. The heat capacity of the empty cell at 1 and 25 kbar plotted as deviations from Eq. (1) with the coefficients fitted to the 1 kbar data.

Fig. 3. The heat capacity of SmS at approximately 15 kbar (triangles), and at zero pressure (circles).

Fig. 4. The heat capacity of the zero-pressure SmS sample in 0 and 38 kOe.

Fig. 5. Estimates of the entropy-change contributions at the transition, and the experimental entropy changes. The curves labelled lattice and d-band electron represent estimates of the lattice and conduction-electronic contributions to ΔS. The curves labelled f^5 and f^6 represent S and -S, respectively, associated with the population of higher energy levels in the $4f^5$ and $4f^6$ multiplets. The curve labelled total represents the sum of the above four contributions, where the last two are weighted by the factor 0.7. The curve labelled experiment is the experimental determination of ΔS up to 20 K between the metallic phase at approximately 15 kbar and the insulating phase at zero pressure. The point at room temperature was calculated from the Claperon equation.

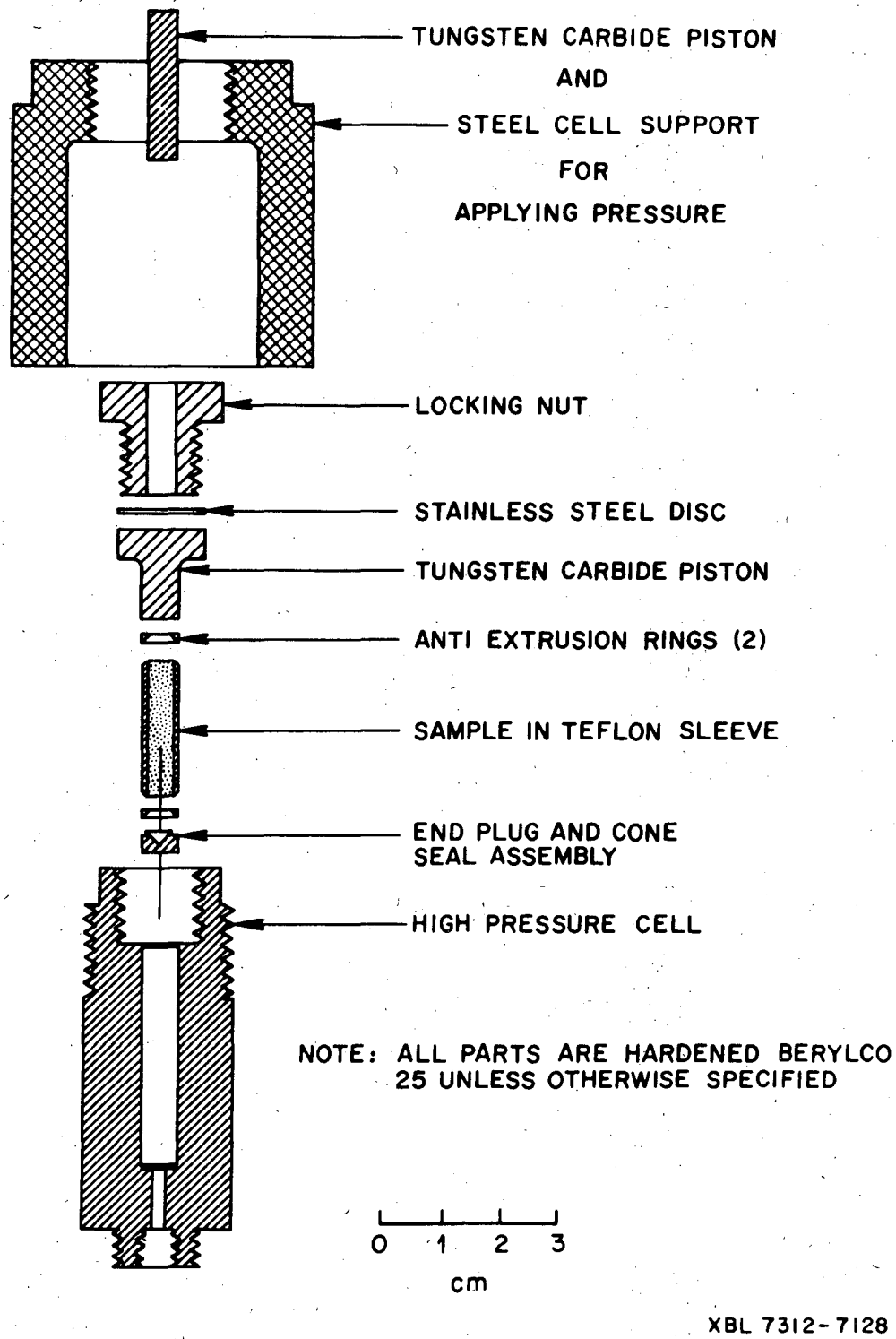
TUNGSTEN CARBIDE PISTON
AND
STEEL CELL SUPPORT
FOR
APPLYING PRESSURE
LOCKING NUT
STAINLESS STEEL DISC
TUNGSTEN CARBIDE PISTON
ANTI EXTRUSION RINGS (2)
SAMPLE IN TEFLON SLEEVE
END PLUG AND CONE
SEAL ASSEMBLY
HIGH PRESSURE CELL
NOTE: ALL PARTS ARE HARDENED BERYLCO
25 UNLESS OTHERWISE SPECIFIED
0 1 2 3
cm
XBL 7312-7128

Fig. III-1.

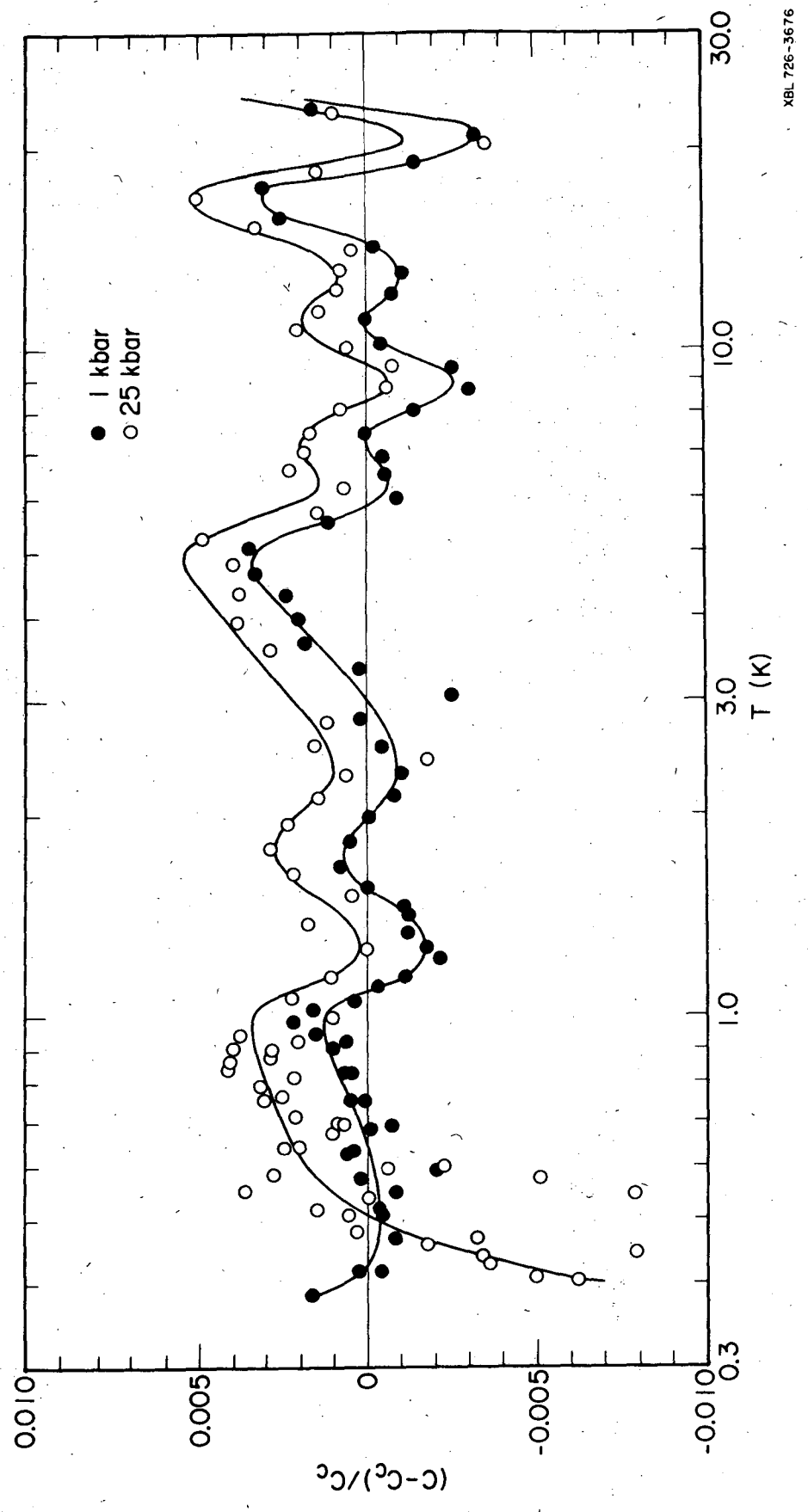
XBL 726-3676
● 1 kbar
○ 25 kbar
0.010
0.005
0
-0.005
-0.010
(C-C_c)/C_c
0.3
1.0
3.0
10.0
30.0
T (K)

Fig. III-2.

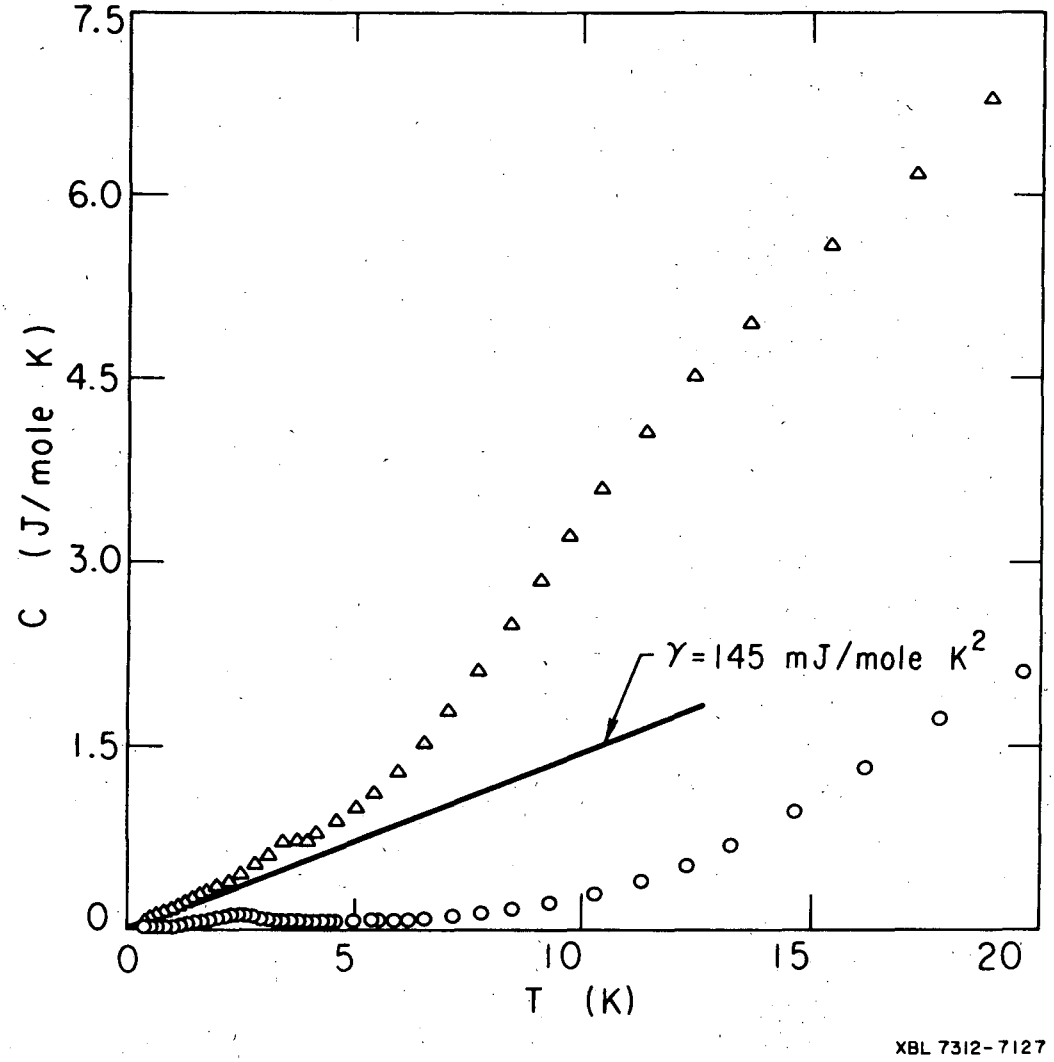
7.5
6.0
4.5
3.0
1.5
0
C (J/mole K)
γ = 145 mJ/mole K²
0
5
10
15
20
T (K)
XBL 7312-7127

Fig. III-3.

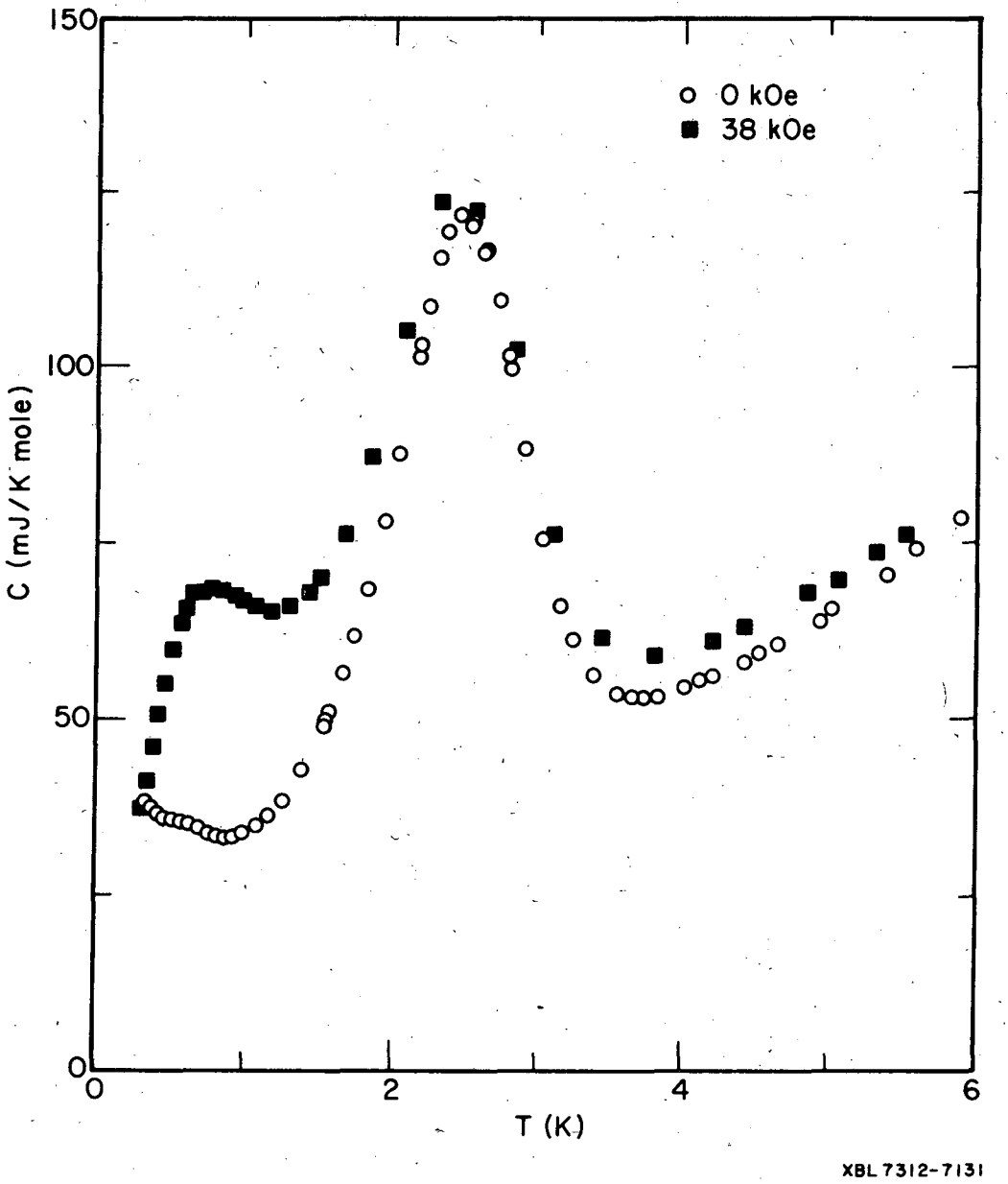

Fig. III-4.

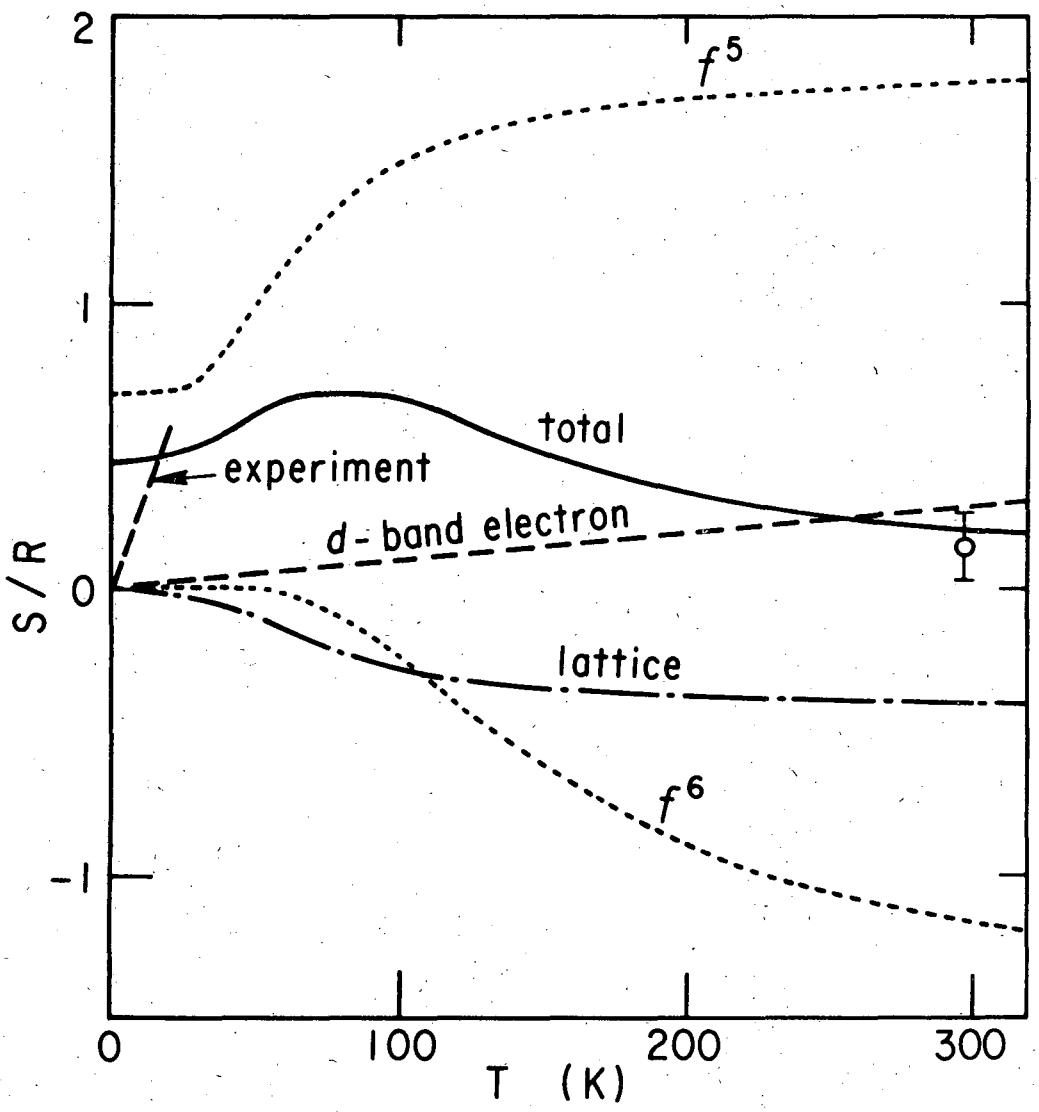

XBL 7312-7126

Fig. III-5.

ACKNOWLEDGMENTS

I wish to thank Professor N. E. Phillips for his guidance, assistance, and advice during these past five years. I wish to express gratitude to Mary Conway, Bill Fogle, Tracy Hall, Jr., Gary Schwartz, Baylor Triplett, and Marilyn Wun, present and former members of this research group, for their numerous contributions.

Professor Leo Brewer has been an inspiration and I would like to thank him for many illuminating discussions. I have had stimulating and rewarding experiences collaborating with Ed Fisher, Brian Maple, and Denis McWhan. I wish to acknowledge fruitful interactions with Gary Brodale, Bob Fisher, Carlos Grahmann, Erwin Hornung, Carlos Luengo, Fred Smith, Whalun Szeto, Dieter Wohlleben. Certain of the samples were either prepared or made available by E. Bucher, T. H. Geballe, and J. M. Schreyer.

I appreciate the assistance of the support staffs of the Chemistry Department and of the Lawrence Berkeley Laboratory. I am especially pleased to acknowledge Carl Baugh, Pearson Kane, Frank Lopez, Dave Milburn, Duane Newhart, George Seiji, Ron Talbot, Wayne Vogen, Don Whittaker, and Hoy Wong, who contributed to the design and construction of new research equipment. Art Peterson and the Metallurgy Department of the Lawrence Livermore Laboratory also provided valuable technical services. Nancy Monroe helped prepared most of the illustrations. Alice Ramirez and Shirley Ashley helped prepare the manuscript in its final form.

I wish also to express sincerest gratitude to all my friends, and to my wife, Karen Natal, and to my mother, Norma Bader.

This work was performed under the auspices of the United States Atomic Energy Commission.

TECHNICAL INFORMATION DIVISION
LAWRENCE BERKELEY LABORATORY
UNIVERSITY OF CALIFORNIA
BERKELEY, CALIFORNIA 94720